Surface reconstruction and derivation of erosion rates over several glaciations (1Ma) in an alpine setting (Sinks Canyon, Wyoming, USA)

Züst, Fabian ; Dahms, Dennis ; Purves, Ross S ; Egli, Markus

Abstract: At middle to high latitudes, many alpine valleys have been shaped by glaciers associated with periods of Pleistocene glaciation. Present glaciated valleys are characterised by broadened valley floors and U-shaped cross sections, continuously formed by glacial activity from initially V-shaped, fluvial cross sections. Sinks Canyon (Wind River Range, USA) is a glaciated valley characterised by a typical U-shaped cross section, containing till from several glacial advances over a range of at least 1 Ma. The morphostratigraphic records indicate a fourfold difference in ice surface elevation between the youngest and oldest glacial periods, which is not easily explained by the present-day valley topography. To assess possible evolution scenarios of Sinks Canyon, we modelled the palaeovalley topography using a geographic information system (GIS) filtering technique in combination with temporal reference points from relative and numerically dated glacial deposits. Ice thicknesses were calculated using the shallow ice approximation. In our model, the valley became shallower and the topography smoother with increasing years back in time. The results suggest that valley topography with ages between 640 and 1000 ka can clearly be distinguished from the present-day topography. Surfaces with ages of 130–200 ka (attributable to MIS 6; Bull Lake glaciation) still could be discerned from present-day topography, but with relatively high uncertainties. The method did not work for topography less than 100 ka or older than 1 Ma. Erosion depths were calculated using the differences between present-day elevation and the modelled surfaces. Calculated erosion rates were within the range of reference values for glacial erosion (0.001 to 1 mm a^{-1}). Glacial erosion appears to have removed 0.52 to 0.72 mm a^{-1} of rock within a time frame of 1 Ma, assuming 200 ka of aggregated glacial flow. If the glacial occupation was longer or the impact of fluvial erosion was not negligible (as assumed), then the calculated rate is lower. If the model assumes a less extended time of glacial flow (b 100 ka), the rate exceeds 1 mm a^{-1}. The method used for surface reconstruction and erosion rates calculation is highly dependent on (i) the reliability of the temporal anchor points and (ii) the assumption of physical glacier conditions (basal shear stress).

DOI: https://doi.org/10.1016/j.geomorph.2014.05.017

Surface reconstruction and derivation of erosion rates over several glaciations (1 Ma) in an alpine setting (Sinks Canyon, Wyoming, USA)

Fabian Züst [a], Dennis Dahms [b], Ross Purves [a], Markus Egli [a,*]

[a] Department of Geography, University of Zurich, CH-8057 Zurich, Switzerland

[b] Department of Geography, University of Northern Iowa, Cedar Falls, USA

* Corresponding author. Tel.: +41 44 635 51 14; fax: +41 635 68 41.

E-mail address: markus.egli@geo.uzh.ch (M. Egli).

Abstract

At middle to high latitudes, many alpine valleys have been shaped by glaciers associated with periods of Pleistocene glaciation. Present glaciated valleys are characterised by broadened valley floors and U-shaped cross sections, continuously formed by glacial activity from initially V-shaped, fluvial cross sections. Sinks Canyon (Wind River Range, USA) is a glaciated valley characterised by a typical U-shaped cross section, containing till from several glacial advances over a range of at least 1 Ma. The morphostratigraphic records indicate a fourfold difference in ice surface elevation between the youngest and oldest glacial periods, which is not easily explained by the present-day valley topography. To assess possible evolution scenarios of Sinks Canyon, we modelled the palaeovalley topography using a geographic information system (GIS) filtering technique in combination with temporal reference points from relative and numerically dated glacial deposits. Ice thicknesses were calculated using the shallow ice approximation.

In our model, the valley became shallower and the topography smoother with increasing years back in time. The results suggest that valley topography with ages between 640 and 1000 ka can clearly

be distinguished from the present-day topography. Surfaces with ages of 130–200 ka (attributable to MIS 6; Bull Lake glaciation) still could be discerned from present-day topography, but with relatively high uncertainties. The method did not work for topography less than ~ 100 ka or older than ~ 1 Ma. Erosion depths were calculated using the differences between present-day elevation and the modelled surfaces. Calculated erosion rates were within the range of reference values for glacial erosion (0.001 to 1 mm a^{-1}). Glacial erosion appears to have removed 0.52 to 0.72 mm a^{-1} of rock within a time frame of 1 Ma, assuming 200 ka of aggregated glacial flow. If the glacial occupation was longer or the impact of fluvial erosion was not negligible (as assumed), then the calculated rate is lower. If the model assumes a less extended time of glacial flow (< 100 ka), the rate exceeds 1 mm a^{-1}. The method used for surface reconstruction and erosion rates calculation is highly dependent on (i) the reliability of the temporal anchor points and (ii) the assumption of physical glacier conditions (basal shear stress).

Keywords: Glaciation; Erosion; Modelling; Pleistocene; Landscape reconstruction

1. Introduction

Pleistocene climate has driven multiple cycles of glacial advance and retreat at middle to high latitudes that have shaped landforms affected by flowing ice (Pierce, 2003; Anderson et al., 2006). During their evolution, glaciated valleys were often occupied by a glacier several times (e.g., Dahms, 2004a; Anderson et al., 2012). Most studies focus on more recent (up to the last 100 ka) or only one glaciation for which the geomorphic evidence seems to be clear. In this paper, we try to reconstruct the surface and to develop a time-split approach for valley wide erosion rates caused by glaciers over 1 Ma that includes several distinct glaciation periods. Although the study of landscapes by mapping and dating morphological and sedimentary features is a long-standing approach to understanding land surface formation (e.g., Dahms, 2004a; Benito-Calvo et al., 2008; Finlayson et al., 2011; Rodríguez-Rodríguez et al., 2011; Trelea-Newton and Golledge, 2012), the

53 overall surface reconstruction is in most cases not possible. Various forward and backward
54 modelling techniques exist that may help to overcome this problem. Such models can either be
55 process- or form-oriented (e.g., Koppes and Montgomery, 2009). Backward modelling using GIS
56 filtering techniques (and combined with numerical dating) seems to be a promising tool to trace
57 back landscape evolution even on a valley scale. This type of model is based more on form
58 development than on process understanding. However, the evolution of landforms can be tracked
59 backward in time, and distinct modelling steps can be correlated with geomorphologic data.
60 Present-day glaciated valleys are characterised generally by broadened valley floors and U-shaped
61 cross sections and are assumed to have been continuously formed by glacial action from initially
62 V-shaped, fluvial cross sections (Harbor, 1992, 1995; Montgomery, 2002; Amerson et al., 2008).
63 The flow of ice on solid bedrock generates glacial erosion as the bedrock is abraded by the ice load
64 as rock fragments slide across it (Huggett, 2003; Amerson et al., 2008). During the advance of a
65 valley glacier, rates of sediment transport are high because of entrained rock slope debris along the
66 valley walls and excavated sediments from the valley floor. Precondition for physical erosion at the
67 glacier's base is a 'warm' glacier bed (Paterson, 1994). Basal sliding velocity, the presence and
68 amount of basal debris, and the movement of englacial debris toward the bedrock are determining
69 factors for erosion intensity. Scour by subglacial meltwater produces channels cut into bedrock
70 under a glacier (Huggett, 2003; Amerson et al., 2008). In a parabolic-shaped valley, the sum of
71 these processes leads to preferential erosion in the valley centre (Harbor, 1992; Fabel et al., 2004;
72 Li et al., 2005; Seddik et al., 2009). Compared to physical erosion, chemical denudation is of minor
73 importance for the evolution of a glaciated valley (Hodson et al., 2000).
74 Sinks Canyon (Wind River Range, Wyoming, USA) is a glaciated valley characterised by a typical
75 U-shaped cross section (Fabel et al., 2004). The canyon contains tills mapped as lateral moraines
76 deposited by glaciers possibly during six glacial periods covering a time frame of at least 1 Ma
77 (Dahms, 2004a). We have the following hypotheses to account for the presence of glacial deposits
78 that span a large elevation gradient in Sinks Canyon:

(A) Glacial erosion changed the valley topography, leading to a valley morphology with a substantially lower average elevation with time (an information that cannot be retrieved from lateral moraines).

(B) The erosion rates during glaciation must have been extraordinarily high.

In addition, the methodological focus of this work implies the following hypotheses:

(C) Reconstruct the evolution of a glaciated valley is possible by use of a topography-based filtering technique with limited input parameters.

(D) Although the reconstruction of the landscape surface has a certain error range, distinguishing surface topographies in the considered time ranges is possible.

To our knowledge, no study has applied a topography-based reconstruction method on a valley scale by combining traditional geomorphologic mapping with relative and numerical dating and a GIS filtering technique to model the valley topography backward in time over several glaciations from the present-day landscape. The intent of our approach is to reconstruct a succession of temporally referenced palaeosurfaces and to calculate related time-split glacial erosion rates.

2. Study area and morphostratigraphic units

Sinks Canyon is a glaciated valley near the south flank of the Wind River Range, a NW-SE–trending massif located in the middle Rocky Mountains of west central Wyoming, USA (Fig. 1). The crest of the range forms nearly 200 km of the United States, western continental divide with 47 peaks above 4000 m (Steidtmann et al., 1989; Dahms, 2002). The range is a Laramide-age structure (~ 60 My) uplifted along the generally NW-SW–trending Wind River thrust fault (Brewer et al., 1982). The uplift tilted the Paleozoic and Mesozoic sedimentary cover to the east. Subsequent erosion exposed the Precambrian crystalline core of the range over an area 175 km long by 45 km wide and created a series of hogbacks and canyons in the Paleozoic/Mesozoic sedimentary units along the east flank of the range (Steidtmann et al., 1989).

105 Sinks Canyon exhibits remnants of a glacial succession that generally corresponds to that
106 previously described for the Wind River Range (Blackwelder, 1915; Richmond, 1986; Hall and
107 Jaworowski, 1999). Additionally, Sinks Canyon contains a record of two older glacial events
108 (younger and older pre-Sacagawea Ridge) that have, to date, no recognised correlates in the Rocky
109 Mountains (Dahms, 2004a). The area of interest covers the main canyon, a 8.5-km-long valley
110 transect bordered by steep valley walls. In addition to the morphostratigraphic units defined by
111 Dahms (2004a; Fig. 2; Table 1), we differentiated the topographic surface within the glaciated
112 valley into separate zones having 'glacial' and 'no glacial' influence and indicators for maximum
113 ice elevation (Fig. 3). Based on field investigations and the detailed geomorphologic descriptions of
114 Dahms (2004a), the altitude of glacial morphological features (moraines, boulders) of five
115 morphostratigraphic units in Sinks Canyon were used to calculate the maximum altitudinal position
116 of the ice surface for each episode in which glacial ice occupied the valley. Morphostratigraphic
117 unit 2 (early Wisconsin) was not used because the ice surface indicators are not clearly
118 distinguishable from the Pinedale limits.
119
120 *Morphostratigraphic unit 1 (unit number according to Dahms, 2004a): Pinedale (MIS 2)*
121 Pinedale (PD) glacial deposits are a complex of five terminal-recessional-lateral moraines along the
122 upper part of the canyon (Dahms, 2004a). Because the early Wisconsin moraines are so closely
123 related to the Pinedale moraines, the early Wisconsin unit was generalised into the Pinedale unit for
124 the purpose of this study. This unit represents the maximum ice extent including recessional stages.
125 The maximum Pinedale valley ice advance is considered to have occurred from 20 to 18 ka BP
126 (MIS 2). It extended to the Sinks leaving a terminal moraine at 1990 m (Gosse et al., 2003; Dahms,
127 2004a,b). Lateral moraines are sharply crested and mark the approximate ice elevation during each
128 recessional stage. Highest moraine crests mark the maximum ice elevation during Pinedale
129 glaciation. The crests are located inside the Bull Lake lateral moraines with an approximate
130 elevation difference of 15 m.

131

132 *Morphostratigraphic unit 3: Bull Lake (MIS 5-6)*

133 Bull Lake (BL) glacial deposits are characterised by more subdued moraine topography than the
134 Pinedale glacial deposits. Lateral moraines are located 15 m above the Pinedale deposits. The
135 longitudinal limit of Bull Lake ice is indicated by a mixture of till and outwash just beyond the
136 mouth of Sinks Canyon at 1805 m (Dahms, 2004a). The corresponding lateral moraines at the
137 mouth also exhibit subdued morphology. Maximum Bull Lake valley glaciation is considered to
138 have occurred between 130 and 200 ka BP and is related to MIS 5–6 (Phillips et al., 1997; Dahms,
139 2004b). The rounded lateral moraine crests mark the maximum elevation of ice during this period.

140

141 *Morphostratigraphic unit 4: Sacagawea Ridge (MIS 16)*

142 The Sacagawea Ridge (ScR) deposits are the oldest glacial remnants identified within and below
143 the canyon rim. In the upper reach of the canyon, these deposits are located ~ 60 to 80 m above the
144 upper limits of Bull Lake moraines. The unit consists of separated patches of moraine deposits
145 having a smoothed topography. The longitudinal limit of Sacagawea Ridge glaciation is marked by
146 an indistinct diamicton beyond the Canyon Mouth that is interpreted as till and outwash of stagnant
147 ice at an elevation of 1760 m (Dahms, 2004a). The Sacagawea Ridge glaciation is estimated to have
148 occurred between 640 and 780 ka BP (MIS 16) (Hall and Jaworowski, 1999; Gosse et al., 2003;
149 Dahms, 2004b). Owing to the barely recognisable morainal topography, the lateral limit of
150 Sacagawea Ridge ice is related to the upper limit of granitic boulders located along the north and
151 south wall of the middle to upper reach of the canyon.

152

153 *Morphostratigraphic unit 5: younger pre-Sacagawea Ridge (>MIS 16)*

154 Younger pre-Sagagawea Ridge (ypScR) deposits are characterised by scattered and isolated
155 diamictons above and beyond the south rim along the lower reach of the canyon and just north of
156 Table Mountain and east of Sawmill Creek (Dahms, 2004a). Remnants are characterised by patches

157 of weathered/shattered boulders on extremely subdued moraines or on Paleozoic bedrock absent
158 surrounding till. Considering the location of these glacial remnants, ice would have extended
159 beyond the lower canyon rim and mouth during glacial occupation (Dahms, 2004a). Two remnants
160 of lateral moraine at the mouth of Sinks Canyon and below the SW end of Table Mountain mark the
161 dimension of the glacier tongue. The younger pre-Sacagawea Ridge glaciation is assumed to have
162 occurred between 730 and 1000 ka BP (Dahms unpublished ^{10}Be exposure ages from granitic
163 boulders). The deposits just beyond the lower reach of the canyon are interpreted as lateral-terminal
164 moraines of a small piedmont lobe. An extensive remnant of till on the wide upland area above the
165 south canyon wall between middle Popo Agie River and Sawmill Creek is characterised by two
166 subdued moraines, indicating the lateral border of ice during glacial occupation. The elevation of
167 the paleo-ice surface is taken from the upper limit of these till remnants, ~ 60 to 80 m above the
168 upper limit of the Sacagawea Ridge deposits.
169
170 *Morphostratigraphic unit 6: older pre-Sacagawea Ridge (>MIS 18)*
171 The older Ppre-Sagagawea Ridge (opScR) unit is described as 'diamicton' (Dahms, 2004a). Love
172 and Christiansen (1985) interpreted the deposits covering Table Mountain as remnant Eocene Wind
173 River Formation, but we use the interpretation of Dahms (2004b) for this deposit consisting of
174 multisized granitic boulders embedded in an unsorted till-like matrix. Dahms interpreted this
175 deposit as a remnant of an earlier Pleistocene glaciation, c. between 1000 and 2500 ka BP. The
176 minimum age estimate is confirmed by preliminary ^{10}Be dating of boulders on the top distal portion
177 of Table Mountain (Dahms, 2004a). Correlated to this main deposit are two small remnants of till
178 behind a prominent rock knob located below and NE of Fossil Hill on the rim of the south eastern
179 canyon wall at c. 2500 m. Maximum ice elevation during the older pre-Sacagawea Ridge glaciation
180 is interpreted as the upper limit of granitic boulders. This suggests a horizontal difference of the ice
181 elevation between younger and older pre-Sacagawea Ridge glaciation of 100 to 150 m.
182

3. Methods

3.1. Topographic modelling approach

The conceptual approach is based on a GIS filtering technique using an adopted approach of Jansson et al. (2010) to model former valley topography. The modelling procedure consists briefly of the following steps:

- Input parameters for the palaeoglaciological landscape reconstruction of Sinks Canyon were obtained from existing studies (geomorphologic map, cosmogenic nuclide dates) and additional field investigations during the summer of 2012.
- Lateral and end moraines served as anchor points for the ice surface.
- The modelled landscape surfaces below the ice were temporally referenced using ice thickness calculations.
- Erosion depths were calculated from the difference between present-day elevation and the modelled surfaces, from which glacial erosion rates were assessed by formulating different scenarios (Fig. 4).

In more detail, the approach is based on neighbourhood analyses that models surfaces using a continuous representation of topography (Jansson et al., 2010). Neighbourhood analysis (or spatial filtering) creates output values for each cell location based on values within a specified neighbourhood, for example calculating a maximum or mean value within such a neighbourhood. The neighbourhood of a central cell is defined by an area of specific form and size (referred to as a kernel), often a square window of 3 x 3 cells, but any other size of window or distance measure is possible (Burrough and McDonnell, 1998). The general equation of a spatial filter to compute a new value of the central cell $C_{i,j}$ within a window is thus:

$$C_{ij} = f\left(\sum_{i-,}^{i+m}\sum_{j-n}^{j+n} c_{ij}\lambda_{ij}\right) \quad (1)$$

where f defines a given operator on windows of sides $2m + 1$, $2n + 1$, and λ_{ij} is a weighting factor (Burrough and McDonnell, 1998). Possible operators f include maximum, minimum, mean, median,

range, standard deviation, sum, or majority.

The model uses an iterative procedure that calibrates model parameters to field evidence of preferential erosion. It has the following steps (Fig. 5):

Module 1: Topographic variable

A DEM with a cell size of 10 m is used (A). Applying block statistics, the maximum value inside a kernel of 3 x 3 cells was extracted and the value assigned to all cells within the kernel (f_1). The resulting raster represents a surface of maximum value blocks with 30 m cell size (B). Again, a smoothed surface was created using a focal mean filter (f_2) to interpolate a new, smoothed DEM, represented by maximum elevation values of the 3 x 3 neighbourhood (C). The calculation of the difference between the input DEM and the new DEM resulted in a grid representing the absolute elevation difference (D). The output of module 1 is a raster containing the difference between the input DEM and surface created by the maximum value extraction.

Module 2: Replication of erosion

Previous works by Harbor (1992) and Fabel et al. (2004) indicated that glacial erosion is most efficient in Sinks Canyon at the valley centre and decreases toward the lateral ice limit. We processed the input grid (D) using a raster calculator to invert each cell value (f_4) so that, for values tending to 0, the limit of the function tends to infinity: $lim_{x \to 0} 1/x = \infty$. Consequently, the value range of the inversion grid is limited to a threshold (maximum erosion) value (f_5). Several tests were carried out in order to (i) calibrate the infill calculations to the erosion depth calculations, (ii) limit the random noise, and (iii) reduce the bias through the introduced value range. The output grid (F) representing a proxy for glacial erosion was added to the input DEM (f_6); this allows the resulting DEM to represent a surface prior to a glacial erosional event (G).

Module 3: Hydrology and topography

In order to avoid small depressions and to ensure hydrological correctness, we post-processed the surface by applying the 'fill' function of the ArcGIS hydrological toolset to fill depressions in the DEM (f_7). To smooth sharp edges resulting from the fill function and the addition of the

topographic variable, we filtered the new surface using a 3 x 3 focal mean filter (f_8). The smoothing of the DEM results in a lowering of exposed surfaces such as ridges or peaks. To avoid surface lowering, cells lower than the input DEM are replaced by the input cell value (f_9). The output DEM represents a surface with equal or higher elevation than the input DEM (J).

Module 4: Glacial geomorphology

The geomorphologic evidence in Sinks Canyon suggests that the ice cover was sequentially less extensive during each successive glacial maximum. The relative zone of glacial influence (= area affected by glacial processes) is defined by a mask of values between 0 for areas outside and 1 for areas inside the zone of glacial influence (f_{10}). Therefore, glacial erosion is only modelled within the zone of glacial influence. The output raster (K) was extracted using a mask limiting the extent of the study area (f_{12}). This raster is the new input DEM for the subsequent model iteration (L).

Module 5: Quantifying erosion

Only the extent of the DEM was considered where geomorphologic evidence suggests the presence of glacial ice. Comparing the higher elevated surface to the initial elevation, the thickness of in-filled material calculated by the filtering procedure was obtained by subtracting the present-day DEM (A_{DEM}) from the output DEM (L_i).

3.2. Paleoglacial ice flow (shallow ice approximation)

The shallow ice approximation (SIA) assesses glacier properties under the assumption of steady state conditions (no change in mass balance) and perfect plastic ice rheology (irreversible deformation without any increase in stress) (Paterson, 1994; Ng et al., 2010). The assumption of perfect plasticity implies that ice deforms in response to the driving stress τ_D, resulting from the weight and surface gradient of the ice. The driving stress is balanced by the basal shear stress τ_B (stress at the contact from glacier ice to bed) that can be interpreted as the yield stress τ_Y for flow to occur. Under the assumption of perfect plasticity, $\tau_Y = \tau_D$, and the yield stress can be expressed as a function of the ice thickness H, the surface slope α, the density of ice ρ, and the gravitational

acceleration g (Hooke, 2005; Benn and Hulton, 2010):

$$\tau_B = \tau_Y = \tau_D = \rho g H \frac{\partial h}{\partial x} \quad (2)$$

with yield stress τ_Y [Pa], ice thickness H [m], density of ice ρ [kg/m^3], gravitational acceleration g [m/s^2], ice surface elevation h [m], and horizontal coordinate x [m]. Ice thickness had to be estimated by the topographic modelling approach. The surface slope α [°] is expressed as:

$$\frac{\partial h}{\partial x} = \tan\alpha \quad (3)$$

In Eq. (1), glacial flow on a plane surface is assumed. This is a reasonable assumption for ice sheets, but is unrealistic for topographically controlled ice masses such as valley and outlet glaciers. In a glacial valley, the valley walls support part of the weight of the glacier, reducing the basal shear stress τ_B compared to the value for a plane surface (Paterson, 1994; Benn and Hulton, 2010). To include this effect, Nye (1952) introduced a correcting shape factor f [-]:

$$\tau_B = \tau_Y = f\tau_D \quad (4)$$

The shape factor is described as a function of the glacier cross section area and tabulated for specific valley forms (Table 2). For a glaciated valley, a parabola is the best approximation (Paterson, 1994). The shape factors are defined as a function of glacier width W [m] and ice thickness H [m] and are tabulated for specific values w.

$$w = \frac{W}{2H} \quad (5)$$

The glacier width could be estimated from the position of the lateral moraines. A shape factor close to 1 indicates a wide, whereas values below 0.5 characterise a narrow, U-shaped valley.

3.3. Ice surface profiles

Ice surface profiles of palaeoglaciers in Sinks Canyon are well documented by lateral moraines, indicating the form of the glacier surface when the glacier was present. When such field evidence is fragmentary, we need to estimate the former ice surface profile. For a glacier resting on a horizontal

bed (e.g., ice sheets or glaciers with a small slope inclination), the variation of glacier thickness H along a flow line can be derived by integrating eq. 5 with respect to x (Nye, 1952; Benn and Hulton, 2010; Ng et al., 2010):

$$H(x) = \left(\frac{2\tau_Y}{\rho g} x \right)^{0.5} \tag{6}$$

The solution is a parabolic curve with the condition that the ice thickness at the edge of the glacier is zero. For an irregular bed, no analytic solution exists and it is necessary to calculate it in a succession of discrete steps (i, $i+1$, $i+2$, …). Equation (5) can be solved numerically by discretising the surface gradient and introducing a specified interval of distance along the x-axis (Δx):

$$\frac{\delta h}{\delta x} = \frac{h_{i+1} - h_i}{\Delta x} \tag{7}$$

Using the spatial discretisation, Eq. (6) can be rewritten:

$$h_{i+1} = h_i + \left(\frac{\tau_Y}{H} \right) \frac{\Delta x}{\rho g} \tag{8}$$

Thereby, the ice thickness can be expressed as $H = h\text{-}B$, where h is the ice surface elevation and B the bed elevation. According to Benn and Hulton (2010), this equation provides an approximate solution of the problem. An exact solution was derived by Van der Veen (1999):

$$h_{i+1}^2 - h_{i+1}(B_i + B_{i+1}) + h_i(B_{i+1} - H_i) - \frac{2\Delta x \bar{\tau}_Y}{\rho g} = 0 \tag{9}$$

The overbar indicates that the yield stress is averaged over the interval. Using the coefficients, the ice surface elevation h was calculated by iterating the glacier along the central flow line and adjusting it to the lateral moraines.

For any relatively homogenous segment of a valley glacier, the basal shear stress tends to be constant (Pierce, 1979; Paterson, 1994). According to Paterson (1994), the typical range of basal shear stress is between 50 and 150 kPa, but values between 25 and 135 kPa are most appropriate for a valley glacier (value of 50 to 150 kPa corrected with a shape factor of 0.5 to 0.9). Because the reconstruction of ice surface profiles is based on the SIA, the application of Eq. (8) to smaller ice bodies like alpine glaciers is limited to gently sloped surface sections (Le Meur et al., 2004).

310 In Sinks Canyon, the glacial succession is well described, mapped, and integrated into the general
311 framework of glacial history of the Rocky Mountains in North America (Pierce, 2003; Dahms,
312 2004a,b). Dahms' existing map of the canyon's glacial deposits was post-analysed to elaborate
313 clearly distinguishable morphostratigraphic units and to integrate indicators for palaeo-ice surface.
314 The map provides the primary input data for the palaeoglaciological characterisation and the
315 temporal referencing of the modelled surface topography.
316 The *maximum zone* and the *relative zones of glacial influence* were compiled by merging the
317 morphostratigraphic units of the glacial deposits into five units including moraines, till, and large
318 granitic boulders that indicate the maximum ice coverage during glacial periods. Glacial erosion
319 rates as a function of valley topography were given by the terrestrial cosmogenic nuclide (TCN)
320 measurements of Fabel et al. (2004). These data served as a base from which to compute the surface
321 stability of the different zones.
322 The present-day boundary of the glaciated valley of Sinks Canyon was defined by the drainage
323 divide taken from the hydrologic unit boundary layer of the sub watershed (12^{th} level for the State)
324 of Wyoming (WyGISC, 2012) and combined with the watershed boundary of Sinks Canyon.
325 During the evolution of Sinks Canyon, the boundary could have changed because of erosion by new
326 incision or the damming effects by ice masses (Hamblin and Christiansen, 2003). The possibility of
327 a different drainage divide is not incorporated and it is assumed to be constant.
328
329 *3.4. Spatial data and software*
330 The palaeosurface reconstruction was performed using a geographic information system (GIS)
331 based on a topographic filtering method in combination with temporal references based on the
332 geomorphologic map and achieved by the calculation of ice surface profiles using the shallow ice
333 approximation (SIA). The direct comparison of the volumetric difference between present-day and
334 modelled topography resulted in the estimation of erosion rates. Figures 4 and 5 provide an
335 overview of the methodological workflow including the main methods, input data, and output

parameters used in the reconstruction. Computation was performed using ArcGIS (ESRI, 1999). All spatial data used for the reconstruction was processed in ArcCatalog and ArcMap software, v10.0. We used ArcScene v10.0 for three-dimensional analysis and display. The main data was accessed from the United States Geological Survey (USGS) and the Wyoming Geographic Information Science Center (WyGISC). All data was integrated in ArcCatalog and projected to the same spatial reference defined by the Universal Transverse Mercator (UTM) system zone 12 with North American Datum (NAD) 83. The native NAD is provided in a geographic coordinate system (USGS, 2013). To use the DEM for terrain analysis, the data set was converted to the UTM zone 12 defined by the NAD 83 using a bilinear interpolation. The projected elevation data (UTM zone 12, NAD 83, 10 m resolution) has a high level of detail suitable for geomorphologic mapping and geomorphometric analysis.

3.5. Topographic filtering using GIS

Based on the present surface topography, a filtering procedure that uses neighbourhood analysis computes the evolution of the surface backward in time, resulting in a representation of an earlier stage of surface development. Using this approach, the valley evolution can be tracked backward in time, offering the possibility to analyze form development and to correlate distinct modelling steps with dated geomorphologic data (Jansson et al., 2010). The 'inversion filtering' method was developed with an iterative procedure that adjusted the filter parameters to empirical data of glacial erosion from TCN measurements in Sinks Canyon (Fabel et al., 2004).

The topography-based filtering method results in surfaces and erosion volumes that are assigned to a number of modelling iterations indicating the relative age but that are not referenced to an absolute time or a timespan. A common method for reconstructing palaeorelief is to identify relict surface remnants for use as anchor points for a reconstructed surface (e.g., Small and Anderson, 1998; Amato et al., 2003; Benito-Calvo et al., 2008). The predicted pattern of topographic evolution can be compared on the valley scale with existing erosion depth measurements (Fabel et al., 2004).

362

363 *3.6. Temporal referencing*

364 Lateral moraines indicate former ice surface elevation (e.g., Finlayson et al., 2011; Hughes et al.,
365 2011). Under the assumption of steady physical properties of a glacier, the modelled valley
366 topography and the interpolated ice surface profile were fit to the Sinks Canyon moraines. The ice
367 rheology and basal sliding conditions (and, thus, the basal shear stress) were assumed to be constant
368 during glaciations for topographically similar valley sections. Using a constant value for the basal
369 shear stress, the ice surface profiles were fit to the valley topography using a spreadsheet program
370 (Benn and Hulton, 2010). Based on palaeoglaciological investigations of the canyon, a basal shear
371 stress value of 35 ± 5 kPa was used (see below, section 4.2). To incorporate the morphological
372 changes in valley cross section, the shape factor was adjusted to each new valley form. All other
373 input parameters were used as defined in the palaeoglaciological characterisation. In the iterative
374 procedure, the reference ice surface profile was fitted to the target elevations (lateral moraines) by
375 increasing the valley elevation. The target elevations were the Bull Lake (BL), Sacagawea Ridge
376 (ScR), and younger pre-Sacagawea Ridge (ypScR) glacial periods. Calculating the difference
377 between temporally referenced palaeosurfaces and present-day topography, the amount and
378 distribution of erosion was calculated and erosion rates assessed using various duration scenarios
379 for ice-occupation of Sinks Canyon.

380

381

382 **4. Results**

383 *4.1. Paleoglaciological characterisation*

384 The terminal position of the end-moraines at the last glacial maximum (LGM; Pinedale) was at
385 1990 m asl and at 1760 m asl at the most extensive ice occupation of the inner canyon (MEG; ScR).
386 Accounting for the maximum elevation of the catchment area (4021 m), the elevation of the
387 equilibrium line altitude (ELA) can be approximated by calculating the mid-range elevation. The

388 ELA range based on the LGM and the MEG extent was ~ 2890–3010 m, which indicates that the
389 part of the glacier flowing through Sinks Canyon was entirely in the ablation zone.
390
391 *4.2. Glaciological parameterisation of ice masses*
392 In a first approximation, the obtained values of basal shear stress were based on the following
393 assumptions and restrictions: that (i) there was no change in valley bottom elevation, (ii) the
394 longitudinal and vertical extent of ice masses occurred approximately synchronous, (iii) the
395 presumably convex cross-sectional ice surface area is approximated as a plane surface, and (iv) the
396 thickness of sedimentary infill of Quaternary age is shallow and thus negligible.
397 The resulting mean basal shear stress in the mid to lower canyon for PD, BL, ScR, ypScR, and
398 opScR are 35, 40, 66 , 120, and 170 kPa, respectively (Table 3). This range of 135 kPa reflects the
399 difference in ice surface elevation of 280 to 300 m between the youngest and oldest documented
400 glaciation (Fig. 6). The main factor of uncertainty is the ice thickness. The indicators of ice surface
401 elevation exhibit a subdued morphology for the older units that gives rise to slight uncertainty of the
402 ice thickness and thus of the basal shear stress calculation. A quantitative assessment remains
403 difficult but is here estimated as a relative error of, at most, 15% of the mean basal shear stress.
404 With the large range of basal shear stress, the question arises if the values are reasonable. Several
405 authors have calculated basal shear stresses for small ice caps and outlet glaciers in and near the
406 Wind River Range for the Pinedale glacial maximum. Locke (1995) analysed physical properties of
407 the icecap covering the northern Rocky Mountains of west-central Montana. For Piedmont lobes
408 advancing 20 km outside the mountain range, values between 10 and 20 kPa were calculated. Pierce
409 (1979) calculated basal shear stress values for the northern Yellowstone outlet glacier, a 50-km-
410 long glacier flowing from the Yellowstone ice cap. Averaged values ranged from 80 and 100 kPa to
411 120 kPa for compressing, uniform, and extending flowing parts, respectively. For a profile crossing
412 Wind River Range from Bull Lake (northeast) to Burnt Lake (southwest), Locke (1995; Montana
413 State University, personal communication, 2013) calculated basal shear stress values of 100 kPa for

414 the inner range and 20 to 45 kPa for the outer end of the glaciers.

415 Based on these modelled values, our calculated values are interpreted as follows: first, the basal
416 shear stress values for the PD, BL, ScR, and ypScR are of the same order of magnitude as reported
417 from other glaciers. Second, when we consider glacier size, the Sinks Canyon valley glacier is a 10-
418 km-long and 0.5- to 1.8-km-wide portion of a palaeoglacier with a total length of 30 km. In
419 contrast, the lobes outside the northern Rocky Mountains and the northern Yellowstone outlet
420 glacier were piedmont lobes approximately three times the size of the Sinks Canyon glacier.
421 Therefore, values reported by Locke (1995; Montana State University, personal communication,
422 2013) most accurately reflect the glacial conditions in Sinks Canyon. This leads to the conclusion
423 that only the calculated basal shear stress values for Pinedale and Bull Lake are in the same range as
424 reported for two other valley glaciers in the WRR. The geomorphologic evidence suggests basal
425 shear stress values for the older glaciations of two to five times higher than the above-noted
426 reference value of 30 to 40 kPa.

427

428 *4.3. Temporally referenced surfaces*

429 Sinks Canyon's former valley topography was modelled using the inversion filtering technique and
430 the temporal references of three glacial periods (BL, ScR, ypScR). The upper valley features a
431 complex topography (Fig. 7). The distal end and upper valley are outside of the area of interest and
432 are only plotted to illustrate the adjacent topography of Sinks Canyon (Figs. 8–10). The basal shear
433 stress is incorporated in the calculations with an estimated error range of ±5 kPa (30–40 kPa; mean
434 value 35 kPa). Because the longitudinal surface characteristic of the distal end and the main canyon
435 is comparable, a constant basal shear stress can be assumed throughout these parts of the valley
436 glacier. The continuous modification of the cross section with continuing model iterations leads to
437 an increased value for the shape factor (see Eq. (4) and Table 2). An overview of the input
438 parameters and number of model iterations is given in Table 4.

439

440 *4.3.1. Bull Lake*

441 An ice surface could be fitted through all target elevations located in the main and upper canyon
442 (Fig. 8). The consideration of the uncertainty in basal shear stress (±5 kPa) leads to a slight bed
443 change. Modelling using the mean (35 kPa) basal shear stress leads to a shallow material infill
444 located mainly along the valley bottom. The longitudinal form is smoothed and irregularities
445 decrease as a consequence of the preferential infill on flat surface reaches of the canyon floor. The
446 reconstruction of the surface during/before Bull Lake glaciation is at the limit of applicability with
447 respect to accuracy. The differences in elevation with the present-day topography are small.

448

449 *4.3.2. Sacagawea Ridge*

450 The morphology modelled for Sinks Canyon during/before the Sacagawea Ridge glaciation (> 640
451 to < 780 ka BP) was substantially different from the present shape of the valley. The surfaces
452 indicate the valley was shallower while the width remained constant (Fig. 9). The uncertainty in
453 basal shear leads to only minor differences in the calculation of the bed elevation. The valley
454 bottom surface is a relatively smooth surface. Compared to the present-day surface, the maximum
455 difference in elevation decreases toward the valley sides. As a result, the cross sections retain the
456 initial U-shape, while the initial valley depth is distinctly reduced. Flat transition zones exhibit
457 terrace-like forms, which we consider to be an artifact of the model technique (CS 87). The shape
458 factor is now increased, which produces a reduction in ice thickness of 10 to 15% for parts of the
459 valley when compared to the Bull Lake glaciation.

460

461 *4.3.3. Younger and older pre-Sacagawea Ridge*

462 The modelled Sinks Canyon valley morphology during/before the younger pre-Sacagawea Ridge
463 glaciation (> 780 to < 1000 ka BP) differs substantially from present-day valley characteristic (Figs.
464 3, 10). Modelling the surfaces during the older pre-Sacagawea Ridge glaciation (ca. 1000 to <
465 2500 ka) was not possible because the geomorphological evidence is too scarce. The model results

466 can be interpreted in three ways:

467 • because the lower target elevations are located along a hillslope at the left side of the
468 canyon, it is possible that hillslope processes led to a displacement of the upper limit of till;
469 • the till was deposited by two independent glacial periods (which would indicate that the
470 moraines between CS 40 and 58 are older than the till near CS 70) and
471 • the till was deposited by the same glaciation, but the valley bottom was more elevated
472 toward the lower end of the canyon.

473 Each of these scenarios seems reasonable, but proof is lacking.

474 The modelled surface elevations demonstrate substantial differences when compared to the present
475 topography. The cross section morphology suggests a flat and shallow valley bottom. In comparison
476 to the present-day valley, the relief is reduced by two-thirds, while the width remains nearly
477 constant. The time period assigned to the younger pre-Sacagawea Ridge glaciation approximates
478 the spatiotemporal limit for the surface reconstruction. Obtaining an accurate model for any higher
479 ice surface (or process area) will be difficult.

480

481 *4.4. Glacial erosion*

482 All time-referenced surfaces exhibit the largest erosion depth at the valley centre with decreasing
483 erosion values toward the side (Fig. 11). The relative error for erosion calculations caused by the
484 variability of basal shear stress decreases with continuing model iterations from 100 to 70% for BL,
485 15% for ScR, and 5% for ypScR. Bull Lake erosion depths are characterised as small patches,
486 whereas the pattern of the erosion depth is more uniform for ScR and ypScR (Fig. 11). The
487 scattered pattern of infill can be attributed to the modelling procedure. The neighbourhood analysis
488 tends to smooth the surface. For the same reason, tributary insections along the canyon walls exhibit
489 increased erosion depths for all time frames. Furthermore, patches of increased erosion along the
490 valley sides (where the initial surface was flat) are present in the upper part of the canyon for ScR
491 and ypScR stages.

492

493 **5. Discussion**

494

495 *5.1. Surface forms*

496 In Sinks Canyon, the modelled difference in ice thickness along a constant longitudinal flow path
497 cannot be explained from the present-day topography. Therefore, hypothesis (A) seems to be
498 correct: glacial erosion has distinctly overprinted the valley's former topography. The inversion
499 filtering method produces a valid pattern of form development over time with the number of
500 glaciations that are assumed to have occupied the canyon (e.g., Harbor, 1992).

501 Over a time range of ~ 1 Ma, the cross section morphology of the canyon developed an increasing
502 flat and wide valley floor. Our reconstructions of the landscape surface were constrained by a
503 sufficient group of anchor points (lateral and end moraines; cf. Fig. 2) to represent each palaeo-ice
504 surface elevation. The differences from the present landscape surface need to be large enough to
505 derive a former surface; consequently, surfaces younger than the BL glaciation could not be
506 distinguished from the modern topography. In contrast, the opScR surfaces could not be
507 reconstructed because of a lack of geomorphic information (although the altitudinal difference
508 between the landscape surfaces certainly seems sufficient). The longitudinal form development of a
509 glaciated valley such as Sinks Canyon is assumed to be a continuous flattening over time
510 (MacGregor et al., 2000). Backward in time, this would imply a slightly steeper valley bottom
511 rather than a flatter one. This assumes that the ice may have been shallower than modelled.

512

513 *5.2. Erosion rates*

514 Benthic oxygen isotope records indicate a fluctuating value of $\delta^{18}O$ that is interpreted as a proxy for
515 climatic conditions and maximum glacial periods. Even though the fluctuations indicate glacial and
516 interglacial periods, it is not possible to assess the duration of the ice coverage for specific
517 locations. Under the assumption that $\delta^{18}O$ data does indeed provide a reliable proxy for glacier

518 extent in alpine valleys, Anderson et al. (2012) approximated the fluctuations using a double sine
519 curve as input for numerical modelling of glacier flow over 10 glacial–interglacial cycles within
520 1 Ma.
521 The time period when ice actually occupied Sinks Canyon is substantially less than the period
522 following the maximum ice extent and the subsequent warm period. The duration of glacial
523 occupation is approximated as a constant fraction of the corresponding time epochs (BL, ScR,
524 ypScR). We calculated three scenarios assuming the duration of ice flow as (i) 20%, (ii) 15% and
525 (iii) 10% of the time represented by each glacial MIS stage (Table 5). These assumptions are
526 supported by other studies comparing the relative efficiency of glacial and fluvial erosion
527 (Montgomery, 2002; Amerson et al., 2008; Anderson et al., 2012). The derived erosion rates are
528 within a plausible range of values when compared to erosion rates calculated for other valley
529 glaciers (Tables 5 and 6) and are within the same order of magnitude as measured for one glacial–
530 interglacial cycle in Sinks Canyon. Taking the calculated erosion rates into consideration, glacial
531 erosion can be considered as one of the most efficient erosive processes in alpine environments
532 (e.g., Hallet et al., 1996; Montgomery, 2002; Brook et al., 2006).
533 One critical uncertainty in modelling remains in the assumption of equal basal shear stress values
534 for different glaciations. Different climatic conditions between the maximum stages could have led
535 to different mass balances, resulting in different ice thicknesses (Haefeli, 1970). Even if the climatic
536 conditions were similar among the glaciations, a continuous lowering of the accumulation area by
537 glacial erosion could have caused a decrease in mass balance, resulting in continuously reduced
538 glacier length (Kaplan et al., 2009; Anderson et al., 2012). However, in Sinks Canyon, the similar
539 longitudinal extent of modelled ice masses over the last ~ 1 Ma suggests similar ice thicknesses,
540 which could only have been influenced by different ice rheologies. Under the assumption of
541 constant basal shear stress, the valley has been lowered to its present elevation by ca. 100 to 110 m
542 with a glacial erosion rate of 0.52 to 0.72 mm a^{-1}, assuming that glacial ice occupied the canyon for
543 200 ka of the last 1 Ma.

544 The range of erosion rates given in Table 6 is based on other studies of comparable methodological,
545 geological, and spatial characteristics. Methods assessing subglacial bedrock erosion are spatially
546 restricted to the channel of glacial flow (or the zone of glacial influence) and seek to quantify the
547 erosive effectiveness of basal processes. The values for in situ abrasion of present-day glaciers
548 range between 1 and 5 mm a^{-1}, but includes only one (abrasion) of several bedrock erosion
549 processes. Differential topographic incision calculations suggest that mean denudation rates here
550 are 0.1–2 mm a^{-1} based on the glacial incision of a preglacial or nonglaciated reference surface. Our
551 derived erosion rate integrates a succession of glacial and interglacial periods over a long time span.
552 Erosion rates that are derived from inherited TCN concentrations in solid bedrock range between
553 0.001 and 0.1 mm a^{-1} and provide site-specific erosion rates that show contrasts in erosion across
554 different landscapes or valley transects (Delmas et al., 2009). Methods to assess the effective rate of
555 glacial erosion include catchment-averaged erosion rates from meltwater sediment fluxes and ice
556 margin sediment volumes that exhibit values of 0.01–10 mm a^{-1} and of 0.001–10 mm a^{-1}
557 respectively. These erosion rates are based on the sediment yield of a catchment area and thus
558 include debris directly eroded by the glacier, debris supplied by supraglacial hillslopes, and
559 sediment from preglacial origin. Thus, the rates cannot be related to specific processes and
560 represent an overall denudation rate of a glaciated catchment (Hallet et al., 1996; Delmas et al.,
561 2009).
562 The reported values of glacial erosion rates in the literature range over four orders of magnitude
563 from 0.001 to 10 mm a^{-1} (Delmas et al., 2009); this is caused by the different types of lithology, the
564 calculation procedure and the high spatial variability of glacial erosion. Furthermore, the time scales
565 over which erosion rates are measured also significantly influence the rates of erosion. Averages of
566 reported denudation rates derived from sediment fluxes or sediment yields decrease by more than
567 an order of magnitude up to two orders of magnitude, respectively, over differing time scales (e.g,
568 from the end of the Little Ice Age, 1–100 years; over glacial–interglacial cycles, > 1 ka; to the entire
569 Quaternary, > 1 Ma) (Koppes and Montgomery, 2009). These extraordinarily high rates are

570 assumed to be a transient response to glacial retreat and are interpreted as paraglacial landscape
571 adjustment (Hallet et al., 1996; Delmas et al., 2009; Koppes and Montgomery, 2009). Over decadal
572 to orogenic time scales, the effective rate of glacial erosion is assumed to range from 0.001 to
573 1 mm a^{-1} (Koppes and Montgomery, 2009).
574 The reconstruction of the morphology of Sinks Canyon considers a topographic incision where the
575 erosion of bedrock was modelled with respect to the zone of glacial influence over a timespan of
576 three glacial periods. The rates reflect glacial erosion and are thus comparable to the erosion rates
577 derived by methods assessing subglacial bedrock erosion covering glacial–interglacial cycles (i.b
578 and i.c; Table 6). When compared to effective rates of glacial erosion, the validity of our model is
579 limited because of the limited spatial reference. Because values from the Wind River Range are
580 available, these values are considered as a good indicator for the order of magnitude.
581 The calculated mean erosion rates (Table 5) of the 130–200, 640–780, and 780–1000 ka time
582 intervals assuming 20% glacial occupation (scenario A) lay between 0.19 and 0.72 mm a^{-1} and,
583 therefore, within the range of the long-term effective erosion rate (0.001–1 mm a^{-1}) over decadal to
584 orogenic time scales (Delmas et al., 2009). Considering scenario B and C, the calculated erosion
585 rates are close to or exceed values reported in literature.
586 Compared to the overall denudation measured in the Wind River Range (Ahnert, 1970; Small and
587 Anderson, 1998), the calculated rates are up to 1 order of magnitude higher. Because the rates are
588 derived from different spatial extents and aggregated processes, a discrepancy in this range is
589 expected (Delmas et al., 2009).
590 Because the measured rates of Ahnert (1970) are averaged over glacial–interglacial periods and
591 glacial erosion is assumed to be more efficient than fluvial erosion (Montgomery, 2002; Brook et
592 al., 2006), the rate during glacial periods is likely to be higher than 0.1 mm a^{-1}. Furthermore,
593 glaciers do not erode equally over the whole glaciated mountain range. Based on modelled glacier
594 flow, Jamieson et al. (2008) suggested an increase in glacial erosion in glacial valleys where the ice
595 is channelled. This can lead to increased erosion rates compared to other parts of the catchment

area, which might be a cause for the large difference in erosion rates between mountain range and valley scale. In Sinks Canyon, erosion measurements from TCN dating over a 20-ka time interval report maximum erosion rates for the valley floor (Fabel et al., 2004; Delmas et al., 2009). Overall, the modelled erosion rates are 2–4 times higher in comparison to the TCN derived rates. Considering the lithological change in Sinks Canyon, the transects used for TCN investigations were within crystalline bedrock; whereas the mid-part of the canyon, where the surfaces were modelled, are predominately characterised by sedimentary rock (sandstone, limestone, dolomite). Compared to crystalline rocks, the sedimentary rocks are less resistant to erosion (Grotzinger et al., 2008), which could lead to a more efficient abrasion in the mid-part of the canyon. Because abrasion is directly coupled to glacial flow velocity (e.g., Harbor, 1992), the flow velocity would need to be equal throughout the whole valley to explain the differences in the varying bedrock lithology. If this was the case, our high erosion rates can possibly be explained by the lithology.

The measured rates in this study are in a similar range (Hebdon et al., 1997; Helgason and Duncan, 2001; Geirsdóttir et al., 2007; Haeuselmann et al., 2007) when compared to studies using a comparable methodological and temporal approach. Helgason and Duncan (2001) and Haeuselmann et al. (2007) found — independent of the topographic location — an abrupt increase in denudation rates in the period 0.8 to 1 Ma BP and hypothesised that numerous climatic changes at this time have influenced glacial flow. Considering one glacial–interglacial cycle, Hebdon et al. (1997) calculated a glacial erosion rate of 2 mm a^{-1} on a comparable lithology. Even though lithological properties vary, glaciated valleys carved into crystalline as well as sedimentary rock feature high erosion rates.

6. Conclusion

We used previously mapped glacial deposits as a time reference for a model of landform evolution within a glaciated valley over a timespan of ~ 1 Ma. This method of temporal referencing is highly dependent on (i) the reliability of the temporal anchor points and (ii) the assumption of physical

622 glacier conditions (basal shear stress).

623 The geomorphic data set of the Sinks Canyon can be considered to be relatively comprehensive
624 with good reliability of the anchor points (Dahms, 2004a,b). Using an inverse filtering technique,
625 we clearly distinguished the earlier valley topography of 640 to 1000 ka from the modern canyon
626 topography (Fig. 7). The ability to calculate the volume of rock or rock debris that is removed
627 within a particular time span and its transformation into a glacial erosion rate is complicated by
628 several factors: (i) the temporal variability of the process, i.e., the timeframe during which the
629 glacier was flowing through the canyon and efficiently eroding material, (ii) the possible
630 contribution of fluvial erosion to the valley incision, (iii) uncertainties in computing the
631 palaeorelief, and (iv) valley infill processes in the past (e.g., rockfalls). Because only the times of
632 maximum glaciations are known, the time frame for 'no ice flow' is only estimated which increases
633 the uncertainty for our calculations. Nonetheless, the calculated erosion rates for Sinks Canyon
634 were within the range of expected values of glacial erosion in the literature. Glacial erosion seems
635 to have removed 0.52 to 0.72 mm a^{-1} of rock in Sinks Canyon within a time frame of 1 Ma,
636 assuming 200 ka of glacial flow.

637 Spatial modelling using the inversion filtering technique and geomorphic mapping clearly showed
638 that glacial erosion strongly influenced the valley's topographic shape. Although the calculations
639 are bound to a certain error, different stages are easily distinguished; however, the method did not
640 work for periods younger than the Bull Lake glaciation (< 125 ka) or older than ~ 1 Ma. The
641 erosion rates (average rates) that we report for glacier activity in Sinks Canyon are relatively high;
642 but the values are in the range of those previously reported in the literature. Our approach enables
643 not only a small-scale resolution of erosion but also the calculation of an average rate over a whole
644 valley.

645

646 **7. Acknowledgements**

We would like to thank two unknown reviewers and Richard A. Marston (editor) for their helpful comments on an earlier version of the manuscript.

References

Ahnert, F., 1970. Functional relationships between denudation, relief, and uplift in large, mid-latitude drainage basins. Am. J. Sci. 268, 243–263.

Amato, A., Aucelli, P.P.C., Cinque, A., 2003. The long-term denudation rate in the Southern Apennines Chain (Italy): a GIS-aided estimation of the rock volumes eroded since middle Pleistocene time. Quatern. Int. 101–102, 3–11.

Amerson, B.E., Montgomery, D.R., Meyer, G., 2008. Relative size of fluvial and glaciated valleys in central Idaho. Geomorphology 93, 537–547.

Anderson, R.S., Molnar, P., Kessler, M.A., 2006. Features of glacial valley profiles simply explained. J. Geophys, Res. 111, 1–14.

Anderson, R.S., Dühnforth, M., Colgan, W., Anderson, L., 2012. Far-flung moraines: Exploring the feedback of glacial erosion on the evolution of glacier length. Geomorphology 179, 269–285.

Benito-Calvo, A., Pérez-González, A., Parés, J.M., 2008. Quantitative reconstruction of Late Cenozoic landscapes: a case study in the Sierra de Atapuerca (Burgos, Spain). Earth Surf. Proc. Land. 33, 196–208.

Benn, D.I., Hulton, N.R.J., 2010. An Excel (TM) spreadsheet program for reconstructing the surface profile of former mountain glaciers and ice caps. Comput. Geosci. 36, 605–610.

Blackwelder, E., 1915. Post-Cretaceous history of the mountains of Central Western Wyoming. J. Geol. 23, 193–217.

Brewer, J.A., Allmendinger, R.W., Brown, L.D., Oliver, J.E., Kaufman, S., 1982. COCORP profiling across the Rocky Mountain Front in southern Wyoming, Part 1: Laramide Structure. Geol. Soc. Am. Bull. 93, 1242-1252.

672 Brook, M.S., Kirkbride, M.P., Brock, B.W., 2006. Quantified time scale for glacial valley cross-
673 profile evolution in Alpine mountains. Geology 34, 637–640.
674 Burrough, P.A., McDonnell, R.A., 1998. Principles of Geographic Information Systems. Oxford
675 University Press, Oxford.
676 Dahms, D.E., 2002. Glacial stratigraphy of Stough Creek Basin, Wind River Range, Wyoming.
677 Geomorphology 42, 59–83.
678 Dahms, D.E., 2004a. Relative and Numeric Age Data for Pleistocene Glacial Deposits and
679 Diamictons in and near Sinks Canyon, Wind River Range, Wyoming, U.S.A. Arct. Antarct. Alp.
680 Res. 36, 59–77.
681 Dahms, D.E., 2004b. Glacial limits in the middle and southern Rocky Mountains, U.S.A., south of
682 the Yellowstone Ice Cap. In: Ehlers, J., Gibbard, P.L. (Eds), Quaternary Glaciations - Extent and
683 Chronology, Part II: North America, Elsevier, Amsterdam, pp. 275–288.
684 Delmas, M., Calvet, M., Gunnell, Y., 2009. Variability of Quaternary glacial erosion rates – A
685 global perspective with special reference to the Eastern Pyrenees. Quaternary Sci. Rev. 28, 484–
686 498.
687 ESRI, 1999. ESRI ArcInfo 10.0 (Redlands, California: ESRI Inc.
688 Fabel, D., Harbor, J., Dahms, D., James, A., Elmore, D., Horn, L., Daley, K., Steele, C., 2004. Spa-
689 tial patterns of glacial Erosion at a valley scale derived from terrestrial cosmogenic ^{10}Be and ^{26}Al
690 concentrations in rock. Ann. Assoc. Am. Geogr. 94, 241–255.
691 Finlayson, A., Golledge, N., Bradwell, T., Fabel, D., 2011. Evolution of a Lateglacial mountain
692 icecap in northern Scotland. Boreas 40, 536–554.
693 Geirsdóttir, Á., Miller, G.H., Andrews, J.T., 2007. Glaciation, erosion, and landscape evolution of
694 Iceland. J. Geodyn. 43, 170–186.
695 Gosse, J.C., Evenson, E.B., Klein, J., Sorenson, C., 2003. Cosmogenic nuclide glacial
696 geochronology in the Wind River Range, Wyoming. In: Easterbrook, D.J. (Ed), Quaternary

Geology of the United States: INQUA 2003 Field Guide Volume, Desert Research Institute, Reno, NV, pp. 49–56.

Haefeli, R., 1970. Changes in the behaviour of the Unteraargletscher in the last 125 years. J. Glaciol. 9, 195–212.

Haeuselmann, P., Granger, D.E., Jeannin, P.-Y., Lauritzen, S.-E., 2007. Abrupt glacial valley incision at 0.8 Ma dated from cave deposits in Switzerland. Geology 35, 143–146.

Hall, R.D., Jaworowski, C., 1999. Reinterpretation of the Cedar Ridge section, Wind River Range, Wyoming: Implications for the glacial chronology of the Rocky Mountains. Geol. Soc. Am. Bull. 111, 1233–1249.

Hallet, B., Hunter, L., Bogen, J., 1996. Rates of erosion and sediment evacuation by glaciers: A review of field data and their implications. Global Planet. Change 12, 213–235.

Hamblin, W.K., Christiansen, E.H., 2003. Earth's dynamic systems 10th edition, Prentice Hall.

Harbor, J.M., 1992. Numerical modeling of the development of U-shaped valleys by glacial erosion. Geol. Soc. Am. Bull. 104, 1364–1375.

Harbor, J.M., 1995. Development of glacial-valley cross-sections under conditions of spatially variable resistance to erosion. Geomorphology 14, 99–107.

Hebdon, N.J., Atkinson, T.C., Lawson, T.J., Young, I.R., 1997. Rate of glacial valley deepening during the Late Quaternary in Assynt, Scotland. Earth Surf. Proc. Land. 22, 307–315.

Helgason, J., Duncan, R.A., 2001. Glacial-interglacial history of the Skaftafell region, southeast Iceland, 0–5 Ma. Geology 29, 179–182.

Hodson, A., Tranter, M., Vatne, G., 2000. Contemporary rates of chemical denudation and atmospheric CO_2 sequestration in glacier basins: an Arctic perspective. Earth Surf. Proc. Land. 25, 1447–1471.

Hooke, R., 2005. Principles of Glacier Mechanics Cambridge University Press, Cambridge.

Huggett, R.J., 2003. Fundamentals of geomorphology. Routledge, London.

722 Hughes, P.D., Woodward, J.C., Van Calsteren, P.C., Thomas, L.E., 2011. The glacial history of the
723 Dinaric Alps, Montenegro. Quaternary Sci. Rev. 30, 3393–3412.
724 Jamieson, S.S.R., Hulton, N.R.J., Hagdorn, M., 2008. Modelling landscape evolution under ice
725 sheets. Geomorphology 97, 91–108.
726 Jansson, K.N., Stroeven, A.P., Alm, G., Dahlgren, K.I.T., Glasser, N.F., Goodfellow, B.W., 2010.
727 Using a GIS filtering approach to replicate patterns of glacial erosion. Earth Surf. Proc. Land. 36,
728 408–418.
729 Kaplan, M.R., Hein, A.S., Hubbard, A., Lax, S.M., 2009. Can glacial erosion limit the extent of
730 glaciation? Geomorphology 103, 172–179.
731 Koppes, M.N., Montgomery, D.R., 2009. The relative efficacy of fluvial and glacial erosion over
732 modern to orogenic timescales. Nat. Geosci. 2, 644–647.
733 Le Meur, E., Gagliardini, O., Zwinger, T., Ruokolainen, J., 2004. Glacier flow modelling: a
734 compari-son of the Shallow Ice Approximation and the full-Stokes solution. CR. Phys. 5, 709–
735 722.
736 Li, Y., Harbor, J., Stroeven, A.P., Fabel, D., Kleman, J., Fink, D., Caffee, M., Elmore, D., 2005. Ice
737 sheet erosion patterns in valley systems in northern Sweden investigated using cosmogenic
738 nuclides. Earth Surf. Proc. Land. 30, 1039–1049.
739 Locke, W.W., 1995. Modelling of icecap glaciation of the northern Rocky Mountains of Montana.
740 Geomorphology 14, 123–130.
741 Love, J.D., Christiansen, A.C., 1985. Geologic Map of Wyoming. Department of the Interior, U.S.
742 Geological Survey, Reston, VA.
743 MacGregor, K., Anderson, R., Anderson, S., Waddington, E., 2000. Numerical simulations of gla-
744 cial-valley longitudinal profile evolution. Geology 28, 1031–1034.
745 Montgomery, D.R., 2002. Valley formation by fluvial and glacial erosion. Geology 30, 1047–1050.
746 Ng, F.S.L., Barr, I.D., Clark, C.D., 2010. Using the surface profiles of modern ice masses to inform
747 palaeo-glacier reconstructions. Quaternary Sci. Rev. 29, 3240–3255.

748 Nye, J.F., 1952. The mechanics of glacier flow. Journal of Glaciology 2, 82–93.
749 Paterson, W.S.B., 1994. Physics of glaciers. Pergamon, Oxford.
750 Phillips, F.M., Zreda, M.G., Gosse, J.C., Klein, J., Evenson, E.B., Hall, R.D., Chadwick, O.A.,
751 Sharma, P., 1997. Cosmogenic ^{36}Cl and ^{10}Be ages of Quaternary glacial and fluvial deposits of
752 the Wind River Range, Wyoming. Geol. Soc. Am. Bull. 109, 1453–1463.
753 Pierce, K.L., 1979. History and dynamics of glaciation in the northern Yellowstone National Park
754 area. U.S. Geological Survey Professional Paper 727 F, 91.
755 Pierce, K.L., 2003. Pleistocene glaciations of the Rocky Mountains. Dev. Quat. Sci. 1, 63–76.
756 Richmond, G.M., 1986. Stratigraphy and correlation of glacial deposits of the Rocky Mountains,
757 the Colorado Plateau and the ranges of the Great Basin. In: Sibrava, V., Bowen, D.Q.,
758 Richmond, G.M. (eds.), Quaternary Glaciations in the Northern Hemisphere, Pergamon Press,
759 Oxford, pp. 99–127.
760 Rodríguez-Rodríguez, L., Jiménez-Sánchez, M., Domínguez-Cuesta, M.J., Rico, M.T., Valero-
761 Garcés, B., 2011. Last deglaciation in northwestern Spain: New chronological and
762 geomorphologic evidence from the Sanabria region. Geomorphology 135, 48–65.
763 Seddik, H., Greve, R., Sugiyama, S., Naruse, R., 2009. Numerical simulation of the evolution of
764 glacial valley cross-sections. arXiv:0901.1177 [physics.geo-ph]
765 Small, E.E., Anderson, R.S., 1998. Pleistocene relief production in Laramide mountain ranges,
766 Western United States. Geology 26, 123–126.
767 Steidtmann, J.R., Middleton, L.T., Shuster, M.W., 1989. Post-Laramide (Oligocene) uplift in the
768 Wind River Range, Wyoming. Geology 17, 38–41.
769 Trelea-Newton, M., Golledge, N.R., 2012. The Younger Dryas glaciation in the southeastern
770 Monadhliath Mountains, Scotland: glacier reconstruction and palaeoclimate implications. Boreas
771 41, 614–628.
772 USGS, 2013. The National Map Viewer and Download Platform
773 (http://nationalmap.gov/viewer.html).

774 Van der Veen, J.W.C., 1999. Fundamentals of glacier dynamics. Balkema, Rotterdam.
775 WyGISC, 2012. Wyoming Geographic Information Science Center WyGISC
776 (http://wygl.wygisc.org/DataServer/).
777
778
779
780
781 **Figure captions**
782
783 Fig. 1. Location of the Sinks Canyon study area in the Wind River Range in west central Wyoming,
784 USA. Sinks Canyon is located at the northeastern end of the Middle Popo Agie valley, 15 km
785 southwest of Lander (data source: WyGISC, 2012; USGS, 2013).
786
787 Fig. 2. Map of Pleistocene glacial deposits in and near Sinks Canyon. The morphostratigraphic units
788 are drawn according to Dahms (2004a). Elevations of contour lines are in metres.
789
790 Fig. 3. Map of process areas defined for Sinks Canyon with respect to previous glaciations. The
791 extent of the glaciated valley is defined by the drainage divide along the southeastern and
792 northwestern valley wall. The zone of maximal glacial influence is defined by the older pre-
793 Sacagawea Ridge glaciation. The partially fragmentary deposits only indicate an approximate
794 extent of ice in the middle part of the canyon; the further extent is uncertain as indicated by
795 question marks. In addition, the different cross sections are indicated by dashed lines. The zone of
796 high stability indicates areas where negligible surface changes have occurred during the last 700 ka.
797
798 Fig. 4. General procedure of the iterative adjustment of the modelled landscape and glacier surface.
799 Starting at the present-day topography, the filtering procedure is applied on the input DEM (*D*). The

800 output is a DEM representing the surface prior to an erosional event (D_t). Out of this surface, the
801 new elevation of the valley centreline is calculated to implement the glacier on the new surface. If
802 the deviation E between the target elevation and the new ice surface does not meet the stop criterion
803 ($E > d_{max}$), the iteration is continued. The iteration procedure is stopped, and the modelled surface
804 temporally referenced (D_t), as soon as the stop criterion meets the minimum deviation ($E < d_{max}$).
805
806 Fig. 5. Flow chart illustrating the inversion filtering method. The present-day DEM is used as input.
807 The modules 1 to 4 show the procedure for one model iteration. The output of the iteration i is a
808 new DEM (L_i). To model a larger erosive impact, multiple iterations are necessary. The number of
809 the iteration i is controlled by the iterator and the output DEM named according to the number of
810 iterations i. MODULE 1 and 2: Neighbourhood analysis was used to extract a variable positively
811 correlated to surface slope for each cell of the raster (D). The inverted value of this variable
812 represents a proxy for the pattern of preferential erosion measured in Sinks Canyon (E). The
813 resulting raster (G) from the addition of raster (F) to the input DEM (A) represents a surface prior to
814 the erosive impact of glacial flow. MODULE 3 and 4: Small depressions are corrected and
815 hydrological correctness was checked by post-processing the DEM using hydrological tools.
816 MODULE 5: Calculation of the difference between the present-day DEM (A_{DEM}) and the output
817 DEM (L_i), the in-filled material was calculated for each cell and evaluated using zonal statistics.
818
819 Fig. 6. Longitudinal ice surface profiles interpolated from glacial remnants of four glacial periods.
820 The distribution of the basal shear stress (mean value) along the valley is plotted in each profile.
821 The large values for steep valley bottom sections show the limitation of the ice surface interpolation
822 based on the SIA. The vertical exaggeration of the profile is 6.
823
824 Fig. 7. Three-dimensional illustration of Sinks Canyon evolution. Present day, Bull Lake (19
825 iterations), Sacagawea Ridge (135 iterations), and younger pre-Sacagawea Ridge (270 iterations)

826 surface topography is illustrated as transparent layer and contour lines of 20-m interval. Moraine
827 crests are indicated as lines for Pinedale (PD), Bull Lake (BL), Sacagawea Ridge (ScR), younger
828 (ypScR) and older pre-Sacagawea Ridge (opScR) periods.
829
830 Fig. 8. Bull Lake longitudinal (LP) and cross-sectional (CS) valley surface. The bed elevation is
831 modelled for three scenarios of basal shear stress (30, 35, 40 kPa). The ice surface at the beginning
832 of Bull Lake (BL) glaciation was fitted through the target elevations and approximated as horizontal
833 line in the cross-sectional plot. The canyon (white background colour) is the area of interest, while
834 the front end and upper valley (grey background colour) are plotted as spatial reference. The
835 vertical exaggeration of the LP is 2.5 and 1.3 for the CS, respectively.
836
837 Fig. 9. Sacagawea Ridge longitudinal (LP) and cross-sectional (CS) valley surface. The bed
838 elevation was modelled for three scenarios of basal shear stress (30, 35, 40 kPa). The ice surface at
839 the beginning of Sacagawea Ridge (ScR) glaciation is fitted through the target elevations and
840 approximated as a horizontal line in the cross-sectional plot. The canyon (white background colour)
841 is the area of interest, while the front end and upper valley (grey background colour) are plotted as
842 spatial reference. The vertical exaggeration of the LP is 2.5 and 1.3 for the CS.
843
844 Fig. 10. Younger pre-Sacagawea Ridge longitudinal (LP) and cross-sectional (CS) valley surface.
845 The bed elevation was modelled for three scenarios of basal shear stress (30, 35, 40 kPa). The ice
846 surface at the beginning of the younger pre-Sacagawea Ridge (ypScR) glaciation is fitted through
847 the target elevations and approximated as a horizontal line in the cross-sectional plot. The canyon
848 (white background colour) is the area of interest, while the front end and upper valley (grey
849 background colour) are plotted as spatial reference. The vertical exaggeration of the LP is 2.5 and
850 1.3 for the CS.
851

852 Fig. 11. Three-dimensional illustration of total (absolute) and iteration step-related (averaged)
853 erosion depth. The total erosion depth was obtained by multiplying the number of model iterations
854 and the corresponding iteration step-related (averaged) value of Bull Lake (19), Sacagawea Ridge
855 (135), and younger pre-Sacagawea Ridge (270). The contour interval is 20 m and represents the
856 interpolated surface of each reference stage.

Table 1

Geomorphologic characteristics of Sinks Canyon morphostratigraphic record (moraine morphology, approximate age, ice limit indication and relative elevation are given for the uppermost indicator and the valley bottom of five described glacial periods in Sinks Canyon) (Phillips et al., 1997; Hall and Jaworowski, 1999; Dahms, 2004a, 2004b)

Unit	Moraine morphology	Age [ka]	Ice limit indication	Rel. elevation[a] [m]
1:Pinedale	sharp crests	18	moraine crest	95
3:Bull Lake	rounded crests; inner margin of moraines are typically covered by Pinedale till	> 130 to < 200	moraine crest	110
4:Sacagawea Ridge	moraine topography barely recognizable	> 640 to < 780	upper limit of granitic boulders; subdued moraine crests	180
5:Younger pre-Sacagawea Ridge	preserved locally only on canyon rims or beyond Canyon Mouth	> 780 to < 1000	upper limit of granitic boulders	245
6:Older pre-Sacagawea Ridge	preserved locally only on canyon rims or beyond Canyon Mouth	> 1000 to < 2500	upper limit of granitic boulders	400

[a] Relative elevation (vertical distance of ice limit indication to valley bottom) estimated from a cross section located between observation point 70 and 75 in the middle part of the canyon with respect to the present-day valley bottom elevation.

Table 2

Shape factor *f* for parabolic valley profiles (values are from Pierce, 1979 and Paterson, 1994)

w	f	w	f
1	0.45	6	0.87
2	0.65	8	0.90
3	0.75	16	0.95
4	0.81	∞	1.00

w = valley form

Table 3

Basal shear stress for five glaciations calculated from present-day glacial morphology (values for PD, BL, ScR and ypScR glaciations were calculated using lateral glacial deposits; the error of the mean basal shear stress is calculated as relative error of 15%)

Glaciation	τ_B mean [kPa]	τ_B max. [kPa]	τ_B min. [kPa]
Pinedale (PD)	35 ± 5	40	30
Bull Lake (BL)	40 ± 6	42	37
Sacagawea Ridge (ScR)	66 ± 10	67	65
Younger pre-Sacagawea Ridge (ypScR)	120 ± 20	140	100
Older pre-Sacagawea Ridge (opScR)[a]	170 ± 25	-	-

[a] Value extrapolated using the modeled ice surface slope from ypScR glaciation.

Table 4

Parameters for the temporal referencing of surfaces; the changing valley cross section shape was incorporated using adjusted shape factors (the different number of iterations for the same reference stage result from the three values of basal shear stress) [a]

Stage	Shape factor [-]	Shear stress [kPa]	Iterations	Comments
BL	0.80	40	0	No iteration necessary; ice surface above TE
		35	19	
		30	33	
ScR	0.85	40	122	
		35	135	
		30	155	TE in main valley used as reference
ypScR	0.90	40	254	
		35	270	Ice surface meets lower TE
		30	280	
opScR	-	-	-	TE out of model range

[a] BL = Bull Lake glaciation: ScR = Sacagawea ridge glaciation: ypScR = younger pre Sacagawea ridge glaciation; opScR = older pre Sacagawea ridge glaciation; TE = target elevation.

Table 5

Glacial erosion rates calculated for BL, ScR, and ypScR glaciation; the rates were calculated using three scenarios (I, II, and III) with different assumptions regarding the duration of glacial flow through the canyon (the duration of glacial flow was estimated using the percent fraction of the reference timespan of each glacial period)

Scenario	Erosion rate [mm/a]		
	Bull Lake (130–200 ka)	Sacagawea Ridge (640–780 ka)	Younger pre-Sacagawea Ridge (780–1000 ka)
A: 20%	0.19–0.30	0.37–0.42	0.52–0.72
B: 15%	0.26–0.40	0.49–0.56	0.70–0.95
C: 10%	0.39–0.60	0.74–0.85	1.05–1.43

Table 6

Compilation of glacial erosion rates (erosion rates for Iceland and Scotland were compiled and calculated by Delmas et al., 2009; the other rates were adopted from the referenced publication if not noted differently)

Region	Spatial reference	Method [a]	Erosion type[b]	Lithology	Interval [ka]	Erosion depth [m]		Erosion rate [mm/a]	Reference
Wind River Range	Mountain range	ii	Den.	Granite	1000		115	0.12	Ahnert (1970)
					1000		100	0.1	Small and Anderson (1998)
Sinks Canyon	Glaciated valley	i.c	Gl.	Granite	20	upper	0.1-3	<0.01–0.15	Fabel et al. (2004) [c]
					20	mid	2-2.5	0.1–0.125	
					20	base	3-12	0.15–0.6	
Iceland	Glaciated valley	i.b	Gl.	Basalt	1000		100	0.1	Geirsdóttir et al. (2007)
					500		200	0.5	
					2200	>0.8 Ma	500	0.23	Helgason and Duncan (2001)
					800	<0.8 Ma	1400	1.75	
Scotland	Glaciated valley	i.b	Gl.	Limestone, sandstone	15		47-68	2	Hebdon et al. (1997)
Switzer-land	Glaciated valley	i.b,c	Gl.	Limestone	1000	<1 Ma	1200	1.2	Haeuselmann et al. (2007)
					1000	>1 Ma	120	0.12	
Sinks Canyon	Glaciated valley	i.b	Gl.	Limestone, sandstone, dolomite	26–40		8	0.19–0.30	this study [d]
					128–146		54	0.37–0.42	
					146–200		105	0.52–0.72	

[a] Method for erosion rate assessment: (ii) sediment mass balance over mountain range; (i.b) differential topographic incision with reference to a benchmark surface; (i.c) TCN dating of glacially eroded bedrock.

[b] Type of erosion rate: denudation (Den.), averaged over the whole time interval and mountain range; glacial erosion (Gl.), averaged over the estimated time interval of glacial flow.

[c] Erosion rate values calculated using a period of glacial occupation of 20 ka instead of 100 ka as used by Delmas et al. (2009) (Fabel, personal communication, 2013); values refer to different valley transects (upper, mid, and base).

[d] Calculated erosion rates refer to scenario A assuming a glacial occupation of 20% of the reference age.

Figure 1

Click here to download high resolution image

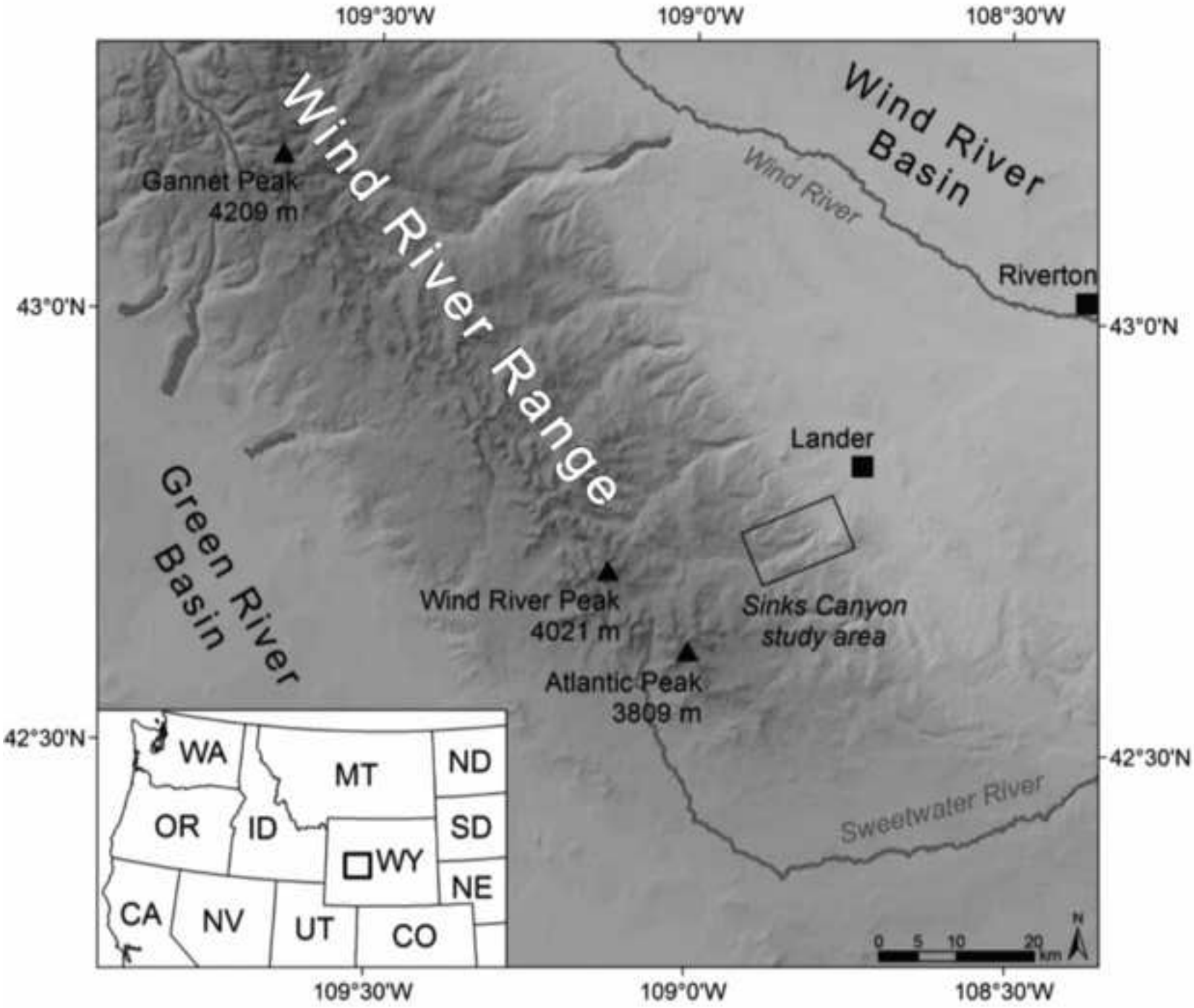

Figure 2

Click here to download high resolution image

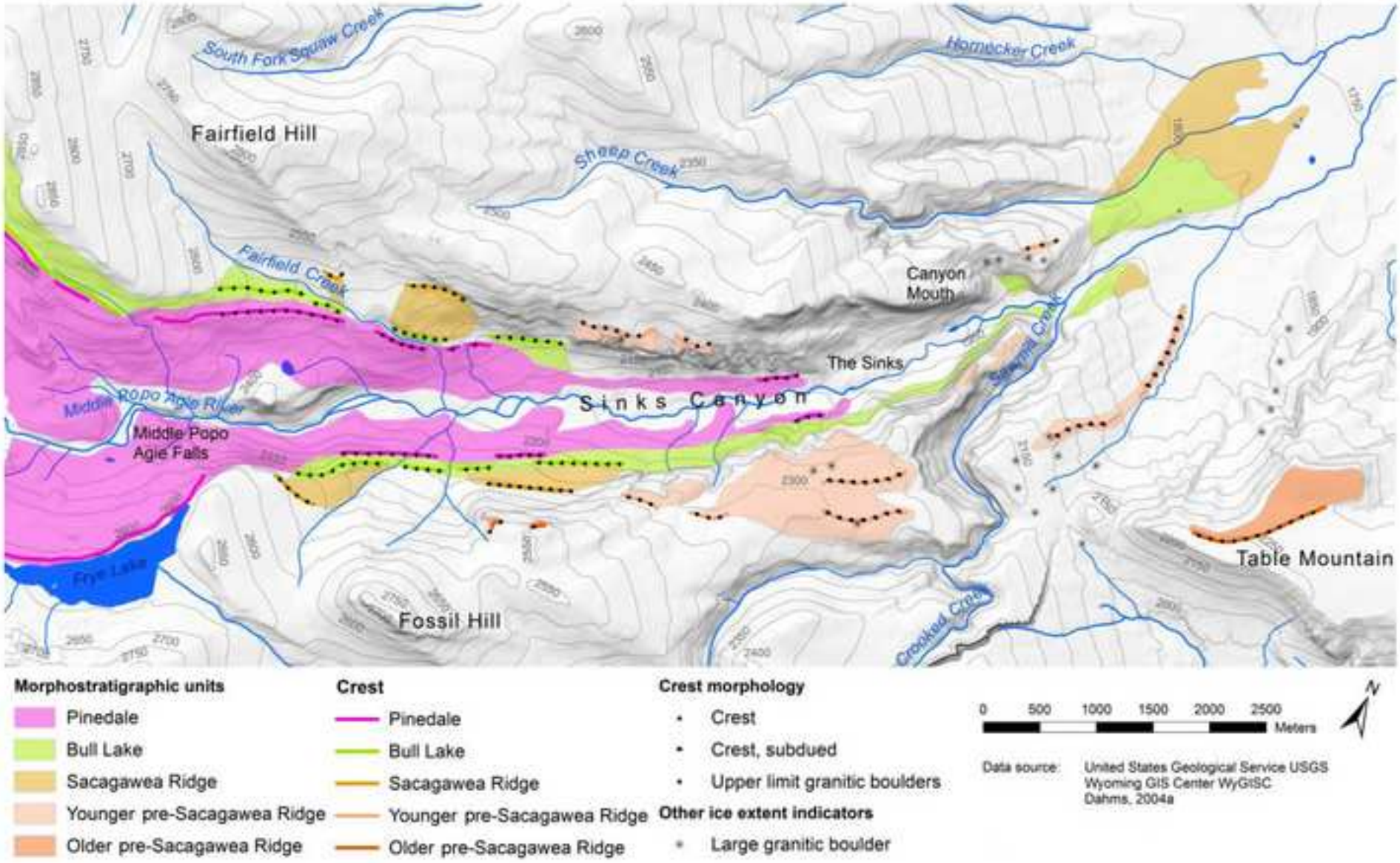

Figure 3

Click here to download high resolution image

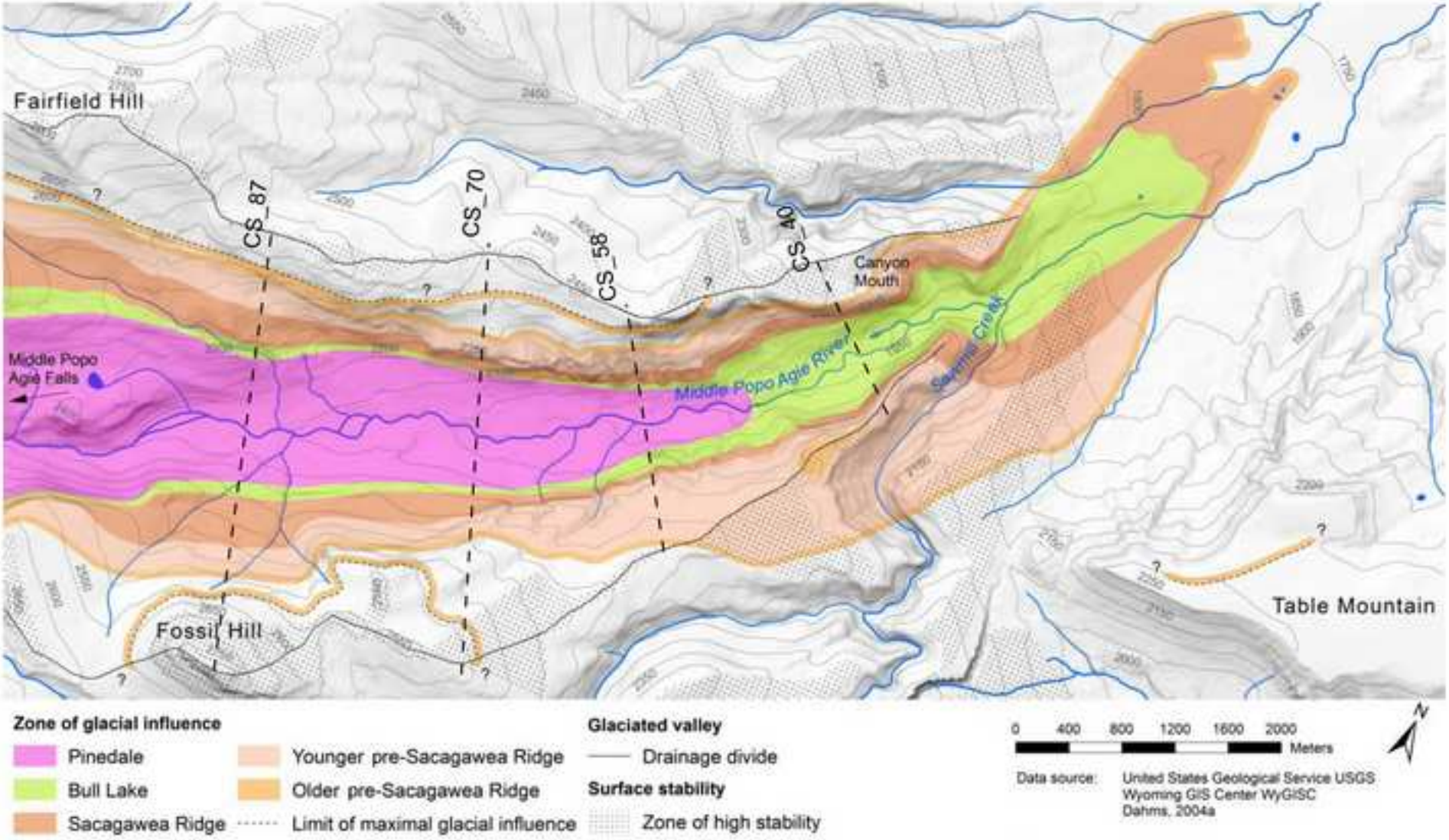

Figure 4
Click here to download high resolution image

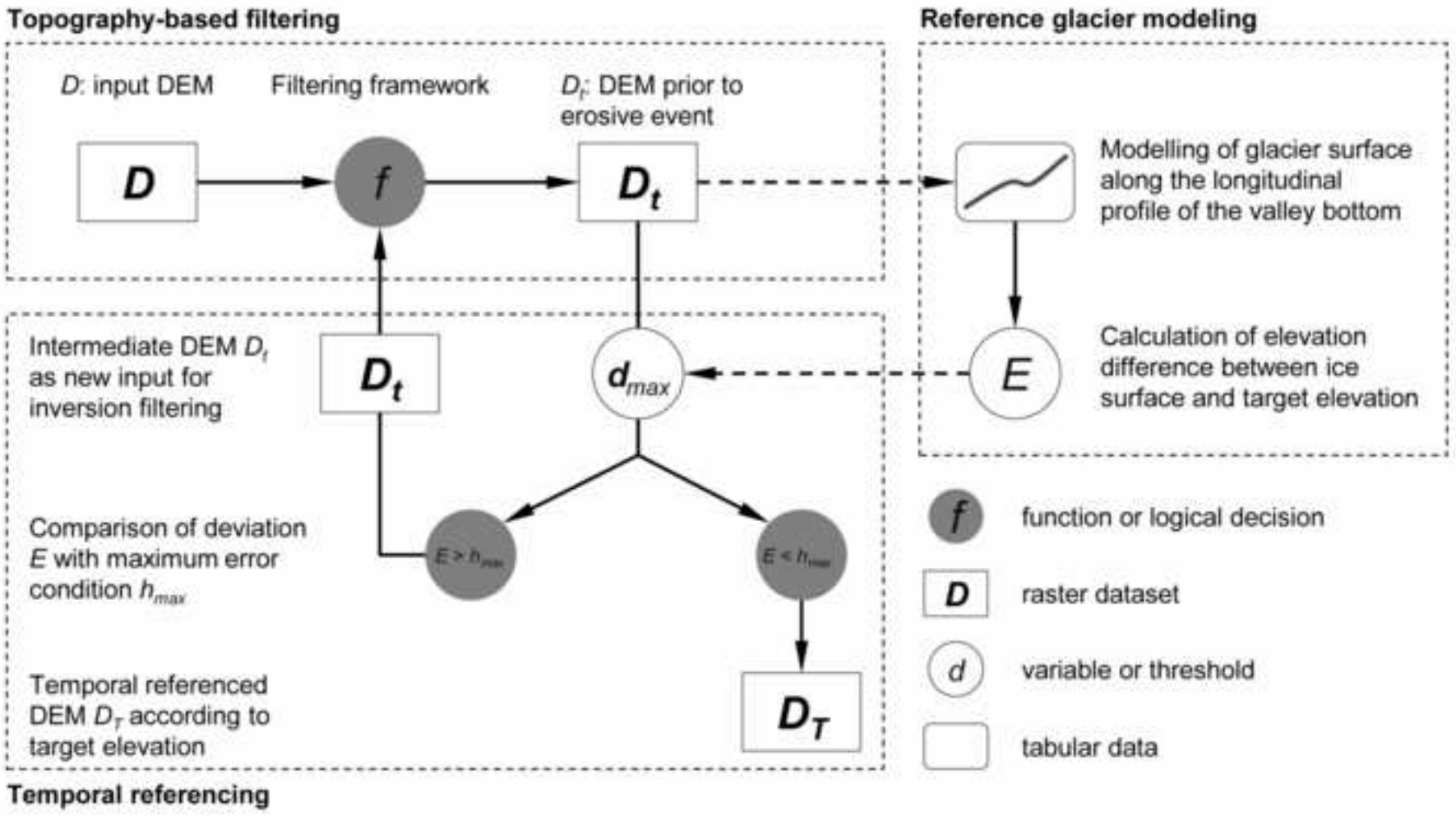

Figure 5

Click here to download high resolution image

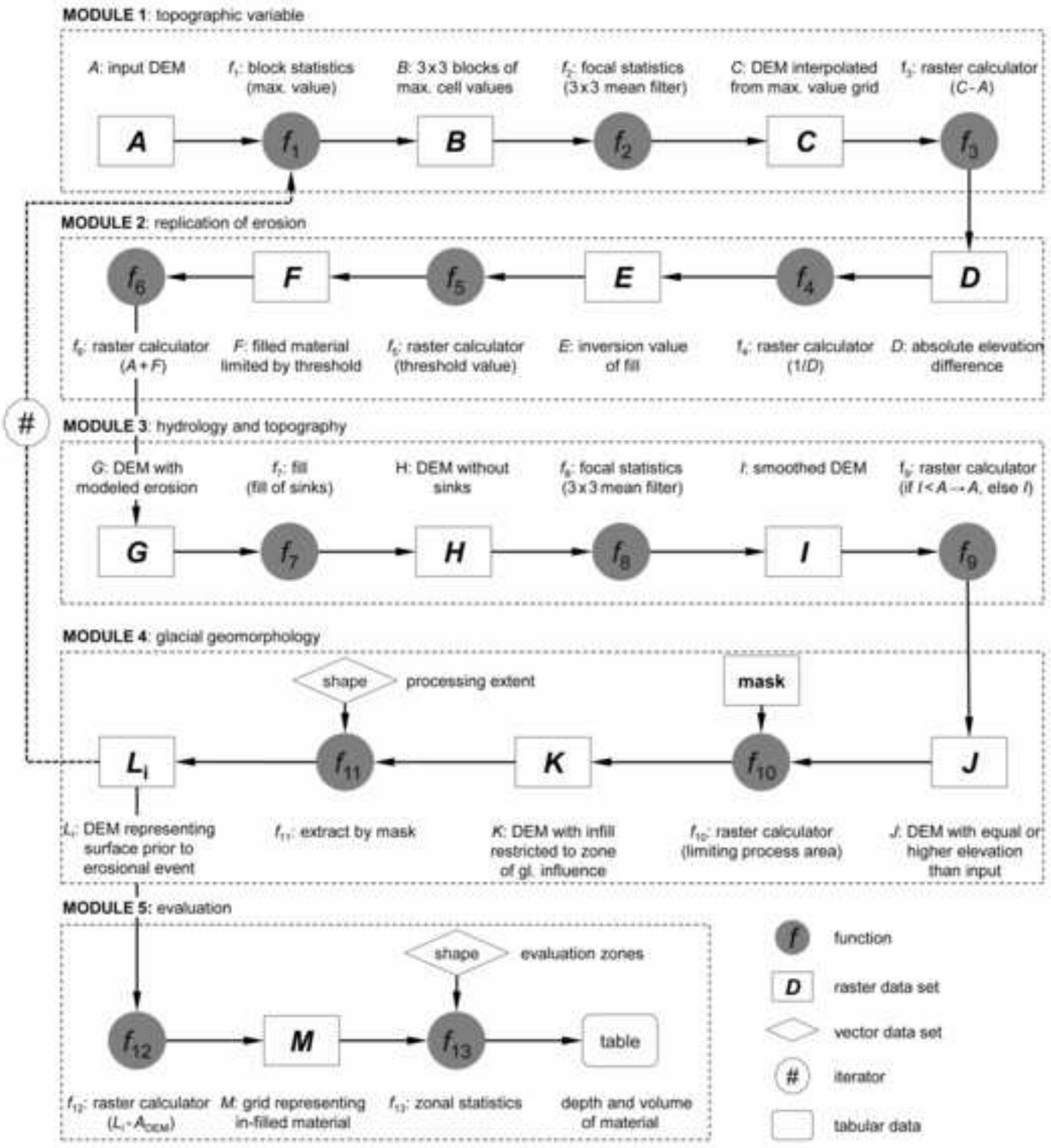

Figure 6

Click here to download high resolution image

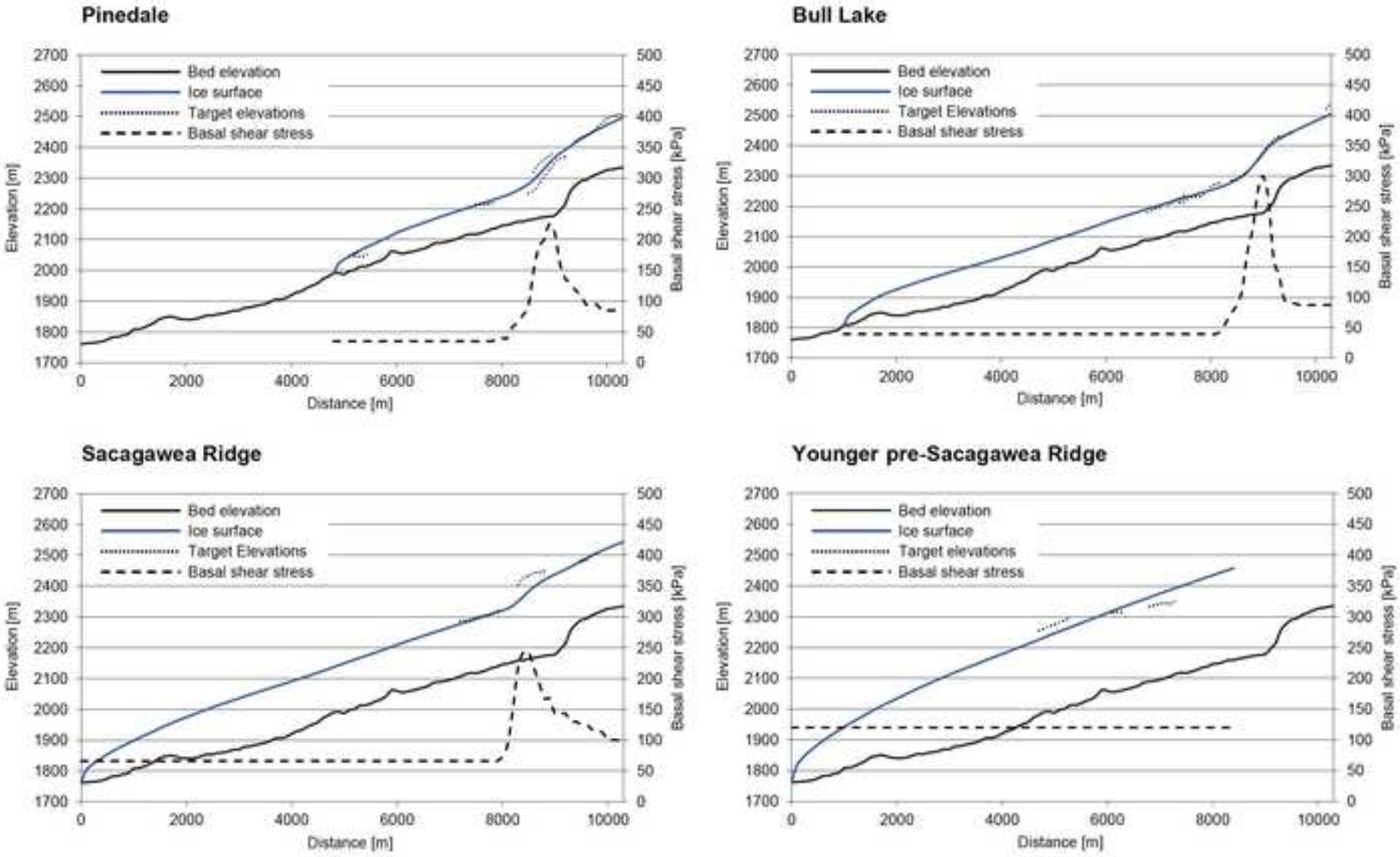

Figure 7

Click here to download high resolution image

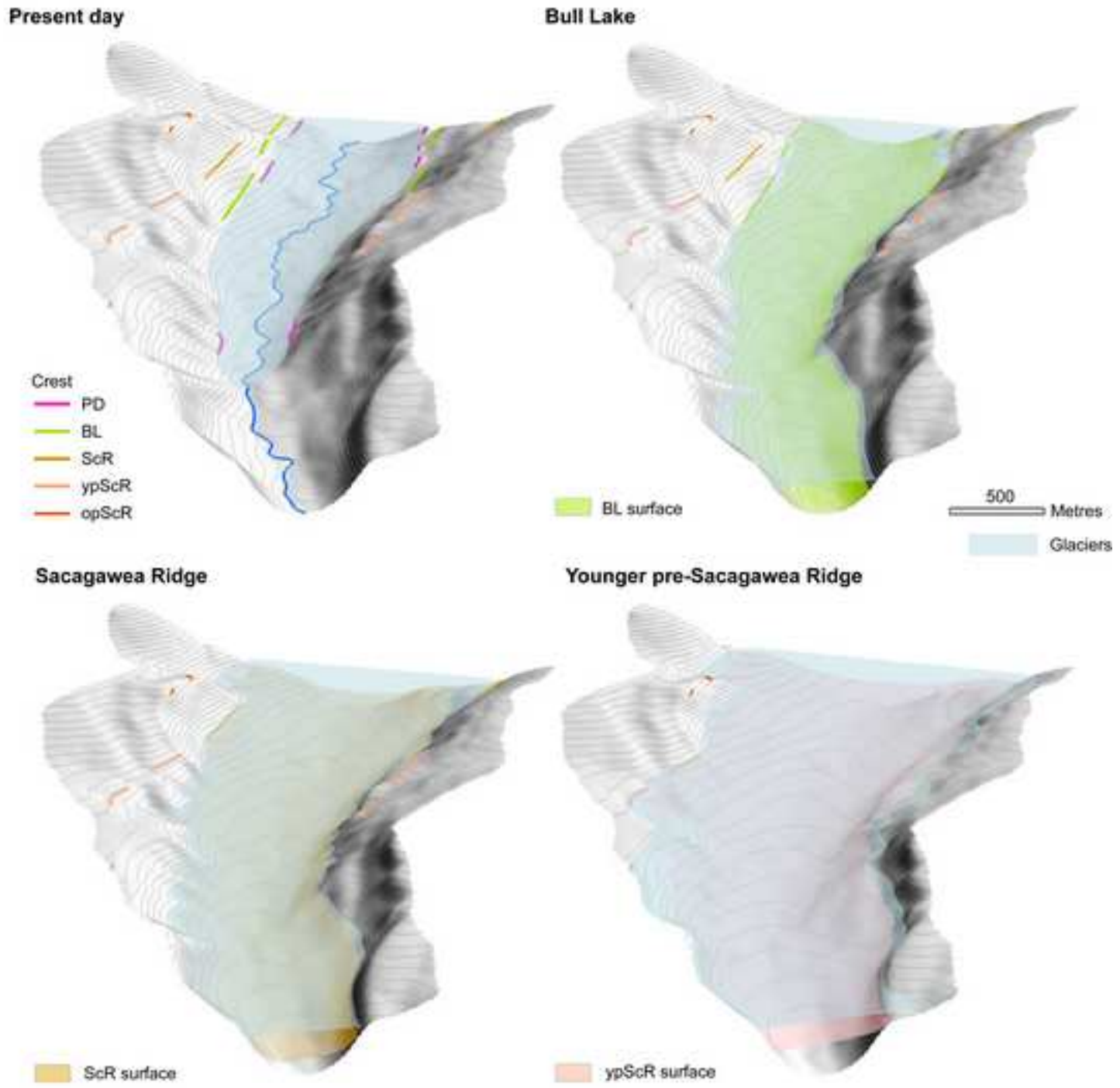

Figure 8

Click here to download high resolution image

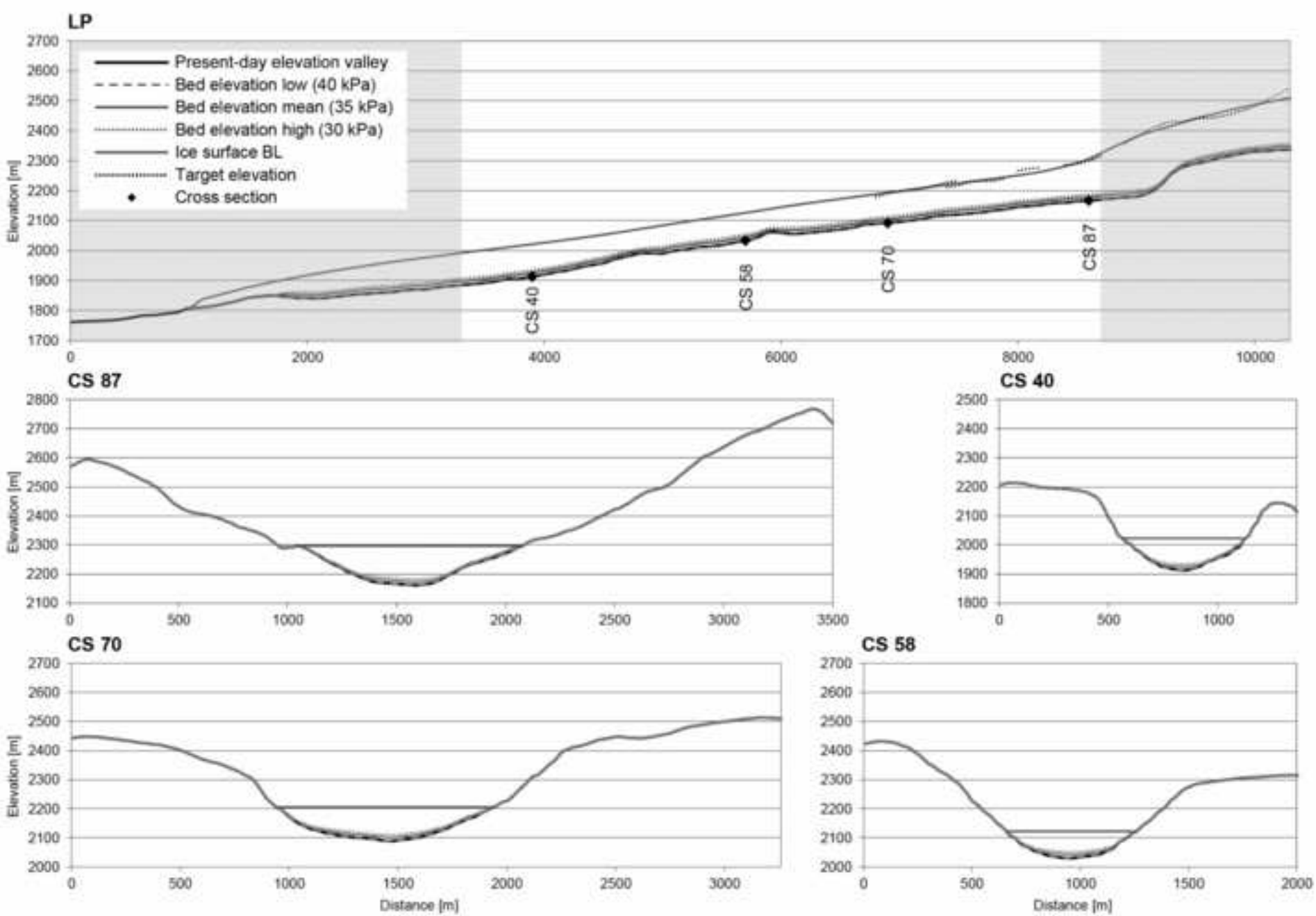

Figure 9

Click here to download high resolution image

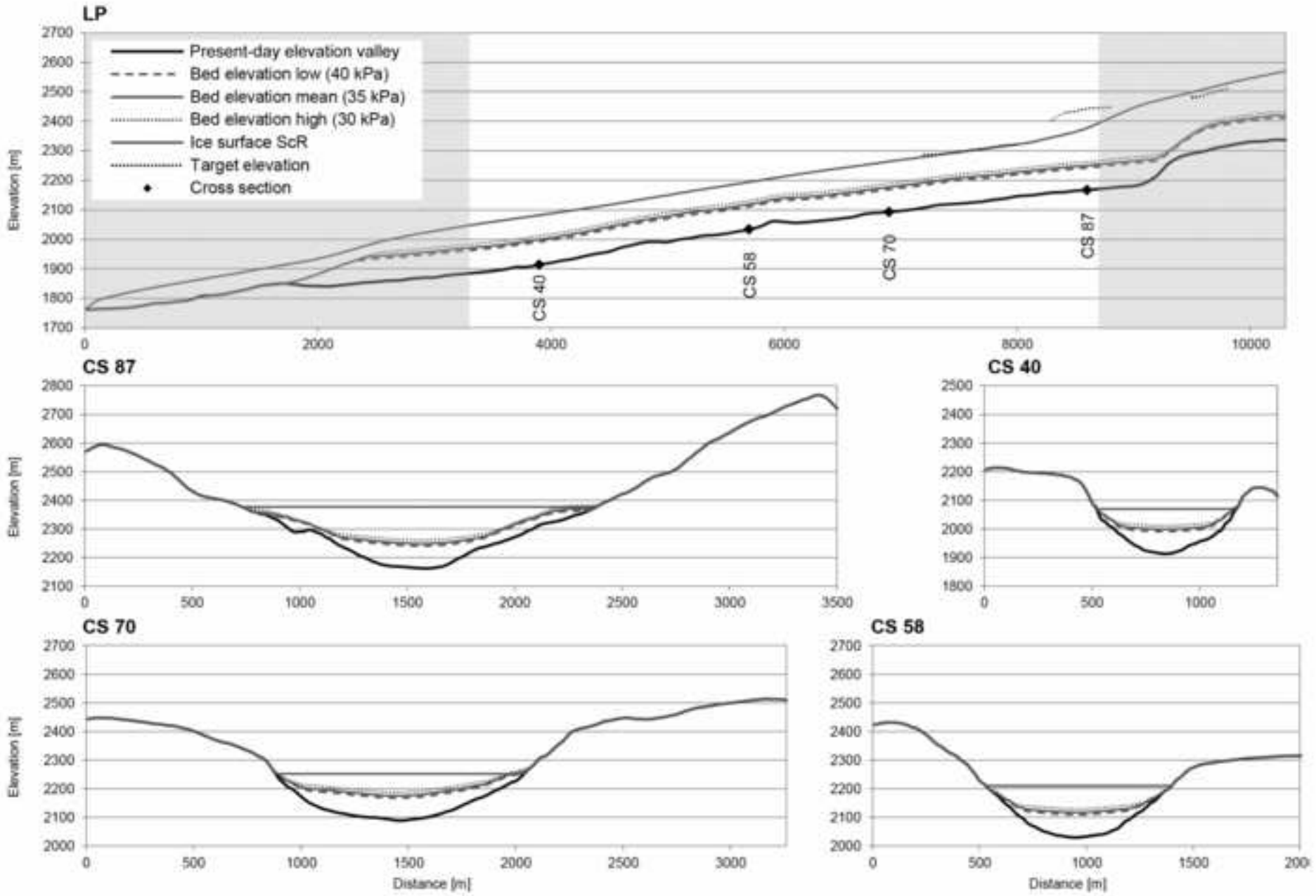

Figure 10

Click here to download high resolution image

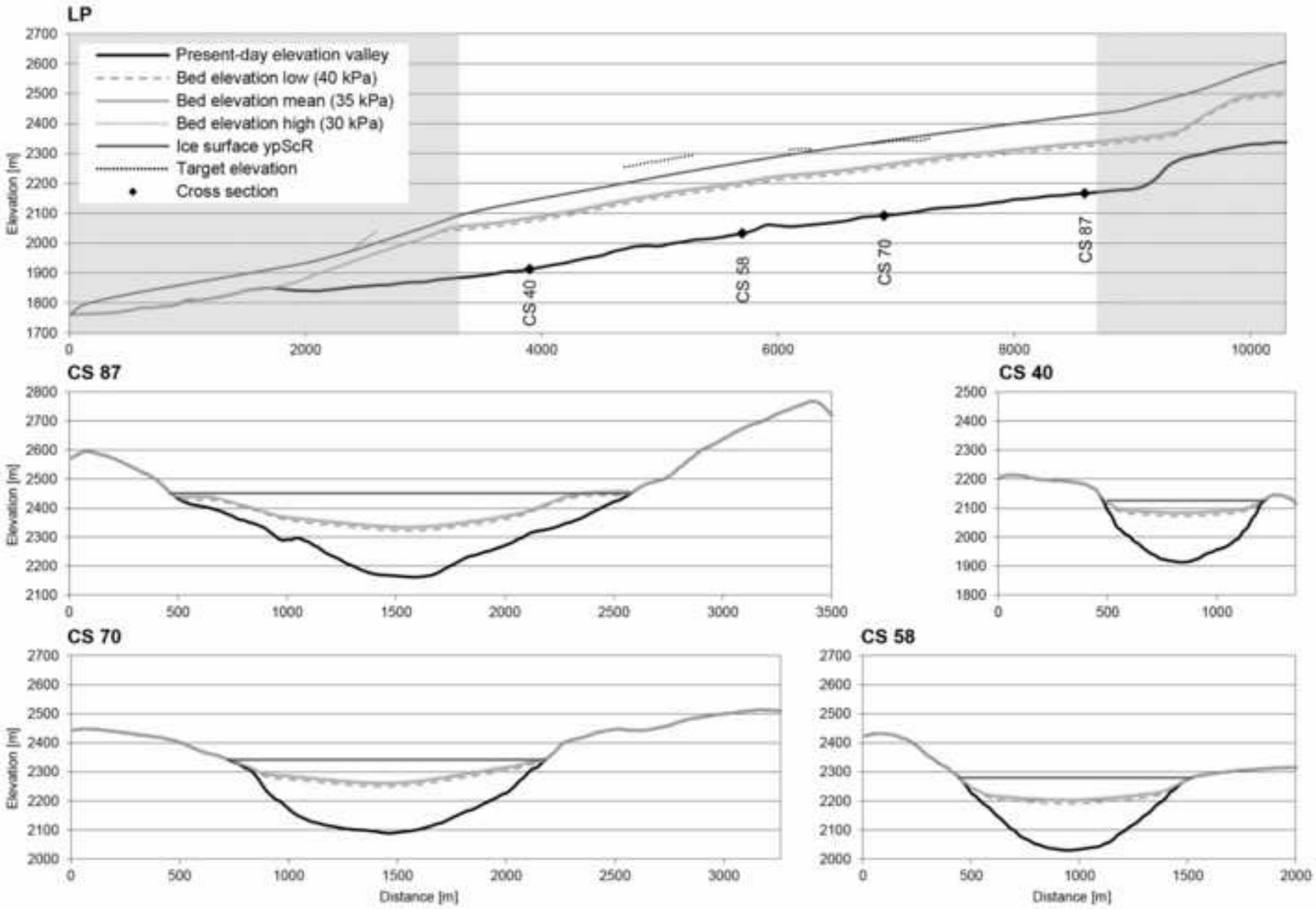

Figure 11
Click here to download high resolution image